

April 11, 2003

U.S. Nuclear Regulatory Commission  
Document Control Desk  
Attn: Mr. Russell Arrighi (Mail Stop O-12D-3)  
Office of Nuclear Reactor Regulation  
Washington, D.C. 20555-0001

Reference: "Request for Additional Information [RAI] for the Review of the R.E. Ginna  
Nuclear Power Plant License Renewal Application [LRA], dated March 21, 2003"


Subject: Response to LRA RAIs 4.2.1-1 and 4.2.2-1  
R. E. Ginna Nuclear Power Plant  
Docket No. 50-244

Dear Mr. Arrighi:

In the referenced letter, RAI 4.2.1-1 requested RG&E to submit the equivalent margin analysis that was performed to demonstrate compliance with the Upper Shelf Energy (USE) requirements of Appendix G to 10CFR50. Enclosure 1 provides the requested report, BAW-2425, Revision 1, "Low Upper-Shelf Toughness Fracture Mechanics Analysis of Reactor Vessel of R. E. Ginna for Extended Life Through 54 Effective Full Power Years", June 2002.

Also in the referenced letter, RAI 4.2.2-1 requested information regarding our use of RG1.190 to perform neutron fluence calculations. Enclosure 2 provides Section 3 of WCAP-15885, Revision 0, "R.E. Ginna Heatup and Cooldown Limit Curves for Normal Operation", July 2002, which describes the radiation analysis and neutron dosimetry used for our reactor vessel calculations.

Very truly yours,

  
Robert C. Mecredy

1000714  
An equal opportunity employer

89 East Avenue | Rochester, NY 14649  
tel (585) 546-2700

www.rge.com

A092

**xc w/enc: Mr. Russ Arrighi, Project Manager  
Office of Nuclear Reactor Regulation  
U.S. Nuclear Regulatory Commission  
One White Flint North  
11555 Rockville Pike  
Rockville, MD 20852**

**xc: w/o enc: Mr. Robert L. Clark (Mail Stop O-8-C2)  
Project Directorate I  
Division of Licensing Project Management  
Office of Nuclear Regulatory Regulation  
U.S. Nuclear Regulatory Commission  
One White Flint North  
11555 Rockville Pike  
Rockville, MD 20852**

**Regional Administrator, Region I  
U.S. Nuclear Regulatory Commission  
475 Allendale Road  
King of Prussia, PA 19406**

**U.S. NRC Ginna Senior Resident Inspector**

**Mr. Denis Wickham  
Sr. Vice President Transmission and Supply  
Energy East Management Corporation  
P.O. Box 5224  
Binghamton, NY 13902**

**LOW UPPER-SHELF TOUGHNESS  
FRACTURE MECHANICS ANALYSIS  
OF REACTOR VESSEL OF R. E. GINNA  
FOR EXTENDED LIFE THROUGH  
54 EFFECTIVE FULL POWER YEARS**

Prepared by

H. P. Gunawardane

VENDOR DESIGN ANALYSIS REVIEW	
<input checked="" type="checkbox"/>	Approved - No Memorandum Required
<input type="checkbox"/>	Approved - Memorandum Attached
<input type="checkbox"/>	Not Approved - Vendor Notified
Approval of this design analysis does not relieve supplier from full compliance with contract or purchase order requirements.	
Approved By	<u>[Signature]</u> Date <u>11/8/02</u>
NS&L Review By	<u>N/A</u> Date _____
(Required if Impact on COLR Values)	
ROCHESTER GAS & ELECTRIC CORP. ROCHESTER, NY	

FRA-ANP Document No. 77-2425-01

Framatome ANP, Inc.  
3315 Old Forest Road  
P. O. Box 10935  
Lynchburg, VA 24506-0935

Category H.66.1  
Reviewed [Signature]


LOW UPPER-SHELF TOUGHNESS  
FRACTURE MECHANICS ANALYSIS  
OF REACTOR VESSEL OF R. E. GINNA  
FOR EXTENDED LIFE THROUGH  
54 EFFECTIVE FULL POWER YEARS

BAW-2425, Rev. 1  
FRA-ANP Document No. 77-2425-01


Prepared for  
Rochester Gas and Electric Corporation

by  
Framatome ANP, Inc.  
Lynchburg, Virginia


This report is an accurate description of the low upper-shelf toughness fracture mechanics analysis performed for the reactor vessel at R. E. Ginna.

  
\_\_\_\_\_  
H. P. Gunawardane, Engineer II                      Date  
Materials and Structural Analysis Unit                      6/12/2002

This report has been reviewed and found to be an accurate description of the low upper-shelf toughness fracture mechanics analysis performed for the reactor vessel at R. E. Ginna.

  
\_\_\_\_\_  
K. K. Yoon, Technical Consultant                      Date  
Materials and Structural Analysis Unit                      6/12/2002

Verification of independent review.

  
\_\_\_\_\_  
A. D. McKim, Manager                      Date  
Materials and Structural Analysis Unit                      6/12/2002

This report is approved for release.

  
\_\_\_\_\_  
J.R. Paljug, Project Development Manager                      Date  
6/12/02

## EXECUTIVE SUMMARY

Since it has been projected that the upper-shelf Charpy energy levels of reactor vessel beltline weld materials at R. E. Ginna may be less than 50 ft-lb at 54 effective full power years of service, a low upper-shelf fracture mechanics evaluation is required to demonstrate that sufficient margins of safety against fracture remain to satisfy the requirements of Appendix G to 10 CFR Part 50.

A low upper-shelf fracture mechanics analysis has been performed to evaluate the SA-847 circumferential reactor vessel weld at R. E. Ginna for ASME Levels A, B, C, and D Service Loadings, based on the evaluation acceptance criteria of the ASME Code, Section XI, Appendix K.

The analysis presented in this report demonstrates that the limiting reactor vessel beltline weld at R. E. Ginna satisfies the ASME Code requirements of Appendix K for ductile flaw extensions and tensile stability using projected low upper-shelf Charpy impact energy levels for the weld material at 54 effective full power years of plant operation.

## RECORD OF REVISIONS

<u>Revision</u>	<u>Affected Pages</u>	<u>Description</u>	<u>Date</u>
0	All	Original release	05/29/02
1	All	Updated analysis to conform to the 1995 Edition of Appendix K to Section XI of the ASME Code, with addenda through 1996. Updated fluence and EFPY values based on latest fluence analysis. Modified copper and nickel content to be consistent with licensing basis.	06/10/02

## CONTENTS

<u>Section</u>	<u>Heading</u>	<u>Page</u>
1.	Introduction .....	1-1
2.	Acceptance Criteria .....	2-1
2.1	Levels A and B Service Loadings (K-2200).....	2-1
2.2	Level C Service Loadings (K-2300).....	2-2
2.3	Level D Service Loadings (K-2400).....	2-2
3.	Material Properties and Reactor Vessel Design Data.....	3-1
3.1	J-Integral Resistance Model for Mn-Mo-Ni/Linde 80 Welds .....	3-1
3.2	Reactor Vessel Design Data .....	3-2
3.3	Mechanical Properties for Weld Material.....	3-3
3.4	J-Integral Resistance for SA-847 Weld Material .....	3-3
4.	Analytical Methodology.....	4-1
4.1	Procedure for Evaluating Levels A and B Service Loadings.....	4-1
4.2	Procedure for Evaluating Levels C and D Service Loadings .....	4-4
4.3	Temperature Range for Upper-Shelf Fracture Toughness Evaluations.....	4-4
4.4	Effect of Cladding Material.....	4-5
5.	Applied Loads .....	5-1
5.1	Levels A and B Service Loadings.....	5-1
5.2	Levels C and D Service Loadings .....	5-1
6.	Evaluation for Levels A and B Service Loadings .....	6-1
7.	Evaluation for Levels C and D Service Loadings.....	7-1
8.	Summary of Results.....	8-1
9.	Conclusion .....	9-1
10.	References.....	10-1
 <u>Appendix</u>		
A.	G. Wrobel (RG&E) letter to J. R. Paljug (FRA-ANP), "RV Parameters," .....	11-1

## LIST OF TABLES

	<u>Page</u>
Table 3-1 Mechanical Properties for Beltline Materials .....	3-2
Table 6-1 Flaw Evaluation for Levels A and B Service Loadings .....	6-2
Table 6-2 $J$ -Integral vs. Flaw Extension for Levels A and B Service Loadings .....	6-3
Table 6-3 $J$ - $R$ Curves for Evaluation of Levels A and B Service Loadings .....	6-4
Table 7-1 $K_I$ vs. Crack Tip Temperature for TPSLB.....	7-5
Table 7-2 $K_{Ic}$ at $1/10$ Wall Thickness .....	7-5
Table 7-3 $K_{Ic}$ at $1/10$ Wall Thickness with $\Delta a = 0.10$ in. ....	7-6
Table 7-4 $J$ -Integral vs. Flaw Extension for Levels C and D Service Loadings.....	7-7
Table 7-5 $J$ - $R$ Curves for Evaluation of Levels C and D Service Loadings.....	7-8
Table 7-6 Level D Service Loadings - Internal Pressure at Tensile Instability .....	7-9

## LIST OF FIGURES

	<u>Page</u>
Figure 1-1 Reactor Vessel Beltline Materials for R. E. Ginna.....	1-2
Figure 2-1 Reactor Vessel Beltline Region with Postulated Longitudinal Flaw .....	2-3
Figure 2-2 Reactor Vessel Beltline Region with Postulated Circumferential Flaw .....	2-4
Figure 5-1 Steam Line Break without Offsite Power transient.....	5-2
Figure 6-1 $J$ -Integral vs. Flaw Extension for Levels A and B Service Loadings .....	6-5
Figure 7-1 $K_I$ vs. Crack Tip Temperature for Levels C and D Service Loadings.....	7-10
Figure 7-2 $J$ -Integral vs. Flaw Extension for Levels C and D Service Loadings.....	7-11



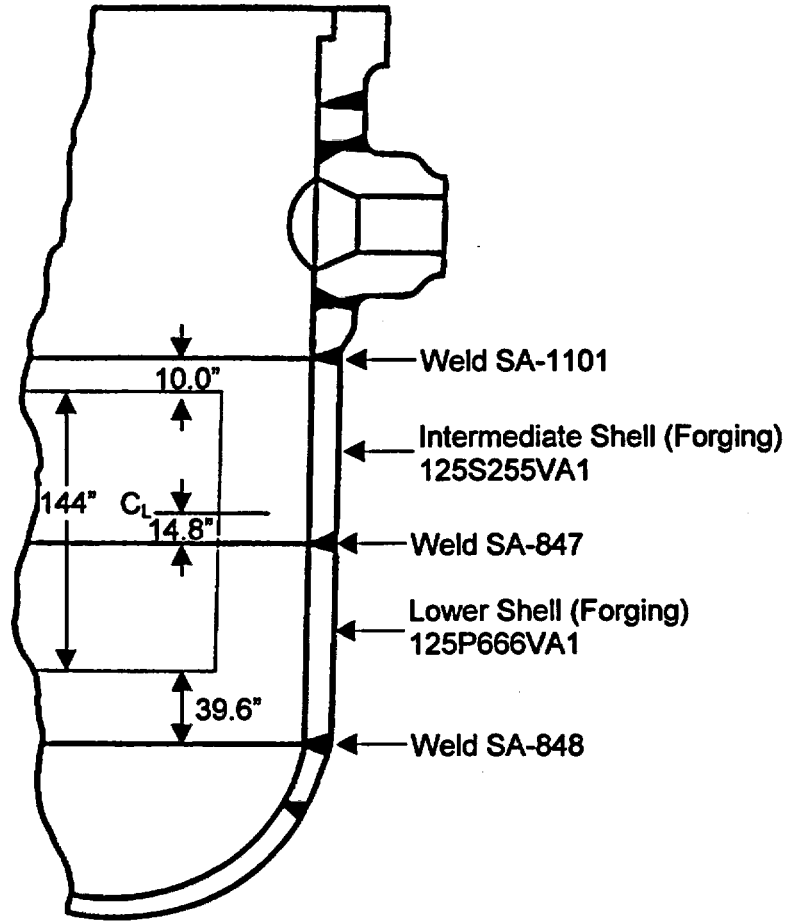
## 1. Introduction

One consideration for extending the operational life of reactor vessels beyond their original licensing period is the degradation of upper-shelf Charpy impact energy levels in reactor vessel materials due to neutron radiation. Appendix G to 10 CFR Part 50, "Domestic Licensing of Production and Utilization Facilities," states in Paragraph IV.A.1.a that, "Reactor vessel beltline materials must have Charpy upper-shelf energy ... of no less than 75 ft-lb initially and must maintain Charpy upper-shelf energy throughout the life of the vessel of no less than 50 ft-lb, unless it is demonstrated in a manner approved by the Director, Office of Nuclear Reactor Regulation, that lower values of Charpy upper-shelf energy will provide margins of safety against fracture equivalent to those required by Appendix G of Section XI of the ASME Code." Materials with Charpy upper-shelf energy below 50 ft-lb are said to have low upper-shelf fracture toughness. Fracture mechanics analysis is necessary to satisfy the requirements of Appendix G to 10 CFR Part 50 for reactor vessel materials with upper-shelf Charpy impact energy levels that have dropped, or that are predicted to drop, below the 50 ft-lb requirement.

The base metal and weld materials used in the beltline regions of the R. E. Ginna reactor vessel are identified in Figure 1-1. Since it has been projected that the upper-shelf Charpy energy levels of the beltline weld materials may be less than 50 ft-lb at 54 effective full power years (EFPY) of service, a low upper-shelf fracture mechanics evaluation has been performed to satisfy the requirements of Appendix G to 10 CFR Part 50. A similar analysis is not required for the reactor vessel beltline forging materials since all applicable materials are predicted to have upper-shelf Charpy energy levels in excess of 50 ft-lb at 54 EFPY.

The present analysis addresses ASME Levels A, B, C, and D Service Loadings. For Levels A and B Service Loadings, the low upper-shelf fracture mechanics evaluation is performed according to the acceptance criteria and evaluation procedures contained in Appendix K to Section XI of the ASME Code [1]. The evaluation also utilizes the acceptance criteria and evaluation procedures prescribed in Appendix K for Levels C and D Service Loadings. Levels C and D Service Loadings are evaluated using the one-dimensional, finite element, thermal and stress models and linear elastic fracture mechanics methodology of Framatome ANP's PCRIT computer code to determine stress intensity factors for a worst case pressurized thermal shock transient.

Figure 1-1 Reactor Vessel Beltline Materials for R. E. Ginna



## 2. Acceptance Criteria

Appendix G to Section XI of the ASME Code [1] provides analytical procedures for the prevention of non-ductile fracture in those areas of the pressure boundary that are comprised of materials with upper-shelf Charpy energy levels of at least 50 ft-lbs. These procedures utilize transition range fracture toughness curves with a fluence-based adjustment to crack tip temperature, and require that the component be operated at a sufficiently low pressure so as to preclude non-ductile failure. These same procedures, however, make no allowance when crack-tip temperatures are maintained above the transition range between cleavage and ductile type failures, where ductile tearing is the predicted mode of failure for ferritic reactor vessel materials. Accordingly, additional evaluation procedures were developed that utilize elastic-plastic fracture mechanics methodology and the concept of J-integral controlled crack growth. Added to Section XI of the ASME Code as Appendix K, these new analytical guidelines may be applied when crack tip temperatures are in the upper-shelf temperature region.

Acceptance criteria for the assessment of reactor vessels with low upper shelf Charpy energy levels are prescribed in Article K-2000 of Appendix K to Section XI of the ASME Code [1]. These criteria, which apply to both longitudinal and circumferential flaws, as depicted in Figures 2-1 and 2-2, respectively, are summarized below as they pertain to the evaluation of reactor vessel weld metals.

### 2.1 Levels A and B Service Loadings (K-2200)

- (a) When evaluating adequacy of the upper shelf toughness for the weld material for Levels A and B Service Loadings, an interior semi-elliptical surface flaw with a depth  $1/4$  of the wall thickness and a length six times the depth shall be postulated, with the flaw's major axis oriented along the weld of concern and the flaw plane oriented in the radial direction. Two criteria shall be satisfied:
  - (1) The applied *J*-integral evaluated at a pressure 1.15 times the accumulation pressure ( $P_a$ ) as defined in the plant specific Overpressure Protection Report, with a factor of safety of 1.0 on thermal loading for the plant specific heatup and cooldown conditions, shall be less than the *J*-integral of the material at a ductile flaw extension of 0.10 in.
  - (2) Flaw extensions at pressures up to 1.25 times the accumulation pressure ( $P_a$ ) shall be ductile and stable, using a factor of safety of 1.0 on thermal loading for the plant specific heatup and cooldown conditions.
- (b) The *J*-integral resistance versus flaw extension curve shall be a conservative representation for the vessel material under evaluation.

### 2.2 Level C Service Loadings (K-2300)

- (a) When evaluating the adequacy of the upper shelf toughness for the weld material for Level C Service Loadings, interior semi-elliptical surface flaws with depths up to  $1/10$  of the base metal wall thickness, plus the cladding thickness, with total depths not exceeding 1.0 in., and a surface length six times the depth,

shall be postulated, with the flaw's major axis oriented along the weld of concern, and the flaw plane oriented in the radial direction. Flaws of various depths, ranging up to the maximum postulated depth, shall be analyzed to determine the most limiting flaw depth. Two criteria shall be satisfied:

- (1) The applied  $J$ -integral shall be less than the  $J$ -integral of the material at a ductile flaw extension of 0.10 in., using a factor of safety of 1.0 on loading.
  - (2) Flaw extensions shall be ductile and stable, using a factor of safety of 1.0 on loading.
- (b) The  $J$ -integral resistance versus flaw extension curve shall be a conservative representation for the vessel material under evaluation.

### 2.3 Level D Service Loadings (K-2400)

- (a) When evaluating adequacy of the upper shelf toughness for Level D Service Loadings, flaws as specified for Level C Service Loadings shall be postulated, and toughness properties for the corresponding orientation shall be used. Flaws of various depths, ranging up to the maximum postulated depth, shall be analyzed to determine the most limiting flaw depth. Flaw extensions shall be ductile and stable, using a factor of safety of 1.0 on loading.
- (b) The  $J$ -integral resistance versus flaw extension curve shall be a best estimate representation for the vessel material under evaluation.
- (c) The extent of stable flaw extension shall be less than or equal to 75% of the vessel wall thickness, and the remaining ligament shall not be subject to tensile instability.

Figure 2-1 Reactor Vessel Beltline Region with Postulated Longitudinal Flaw

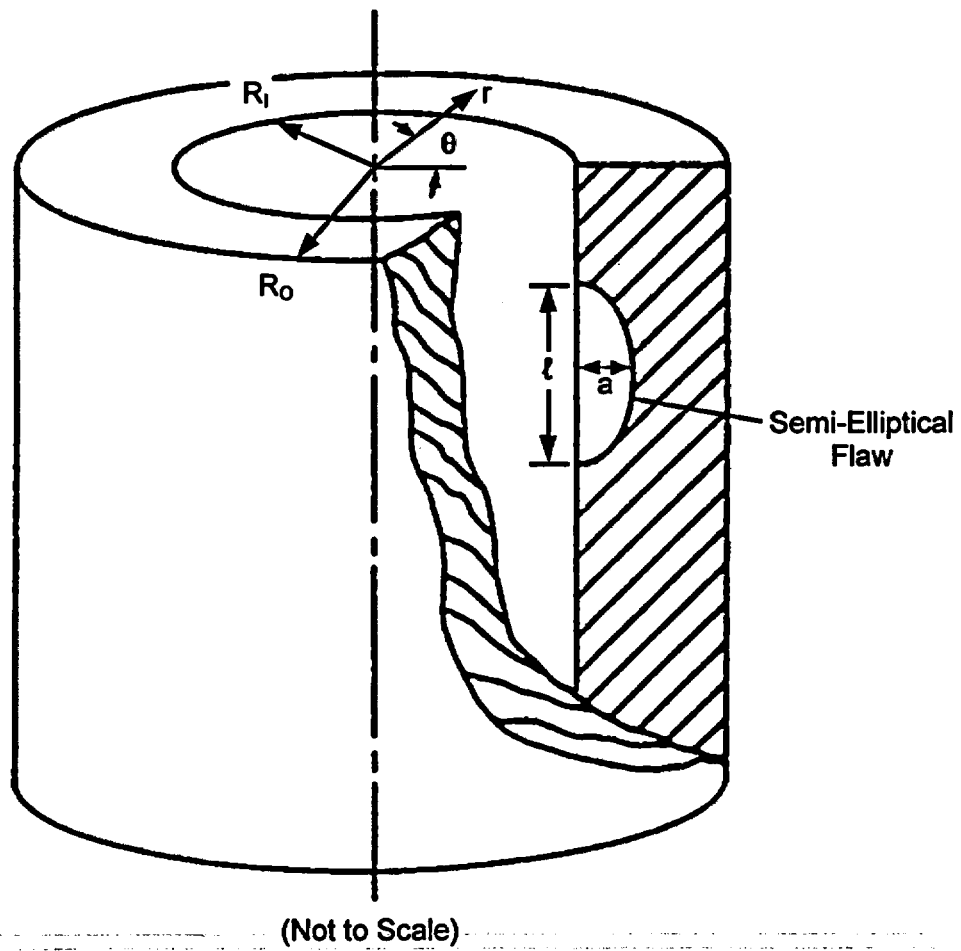
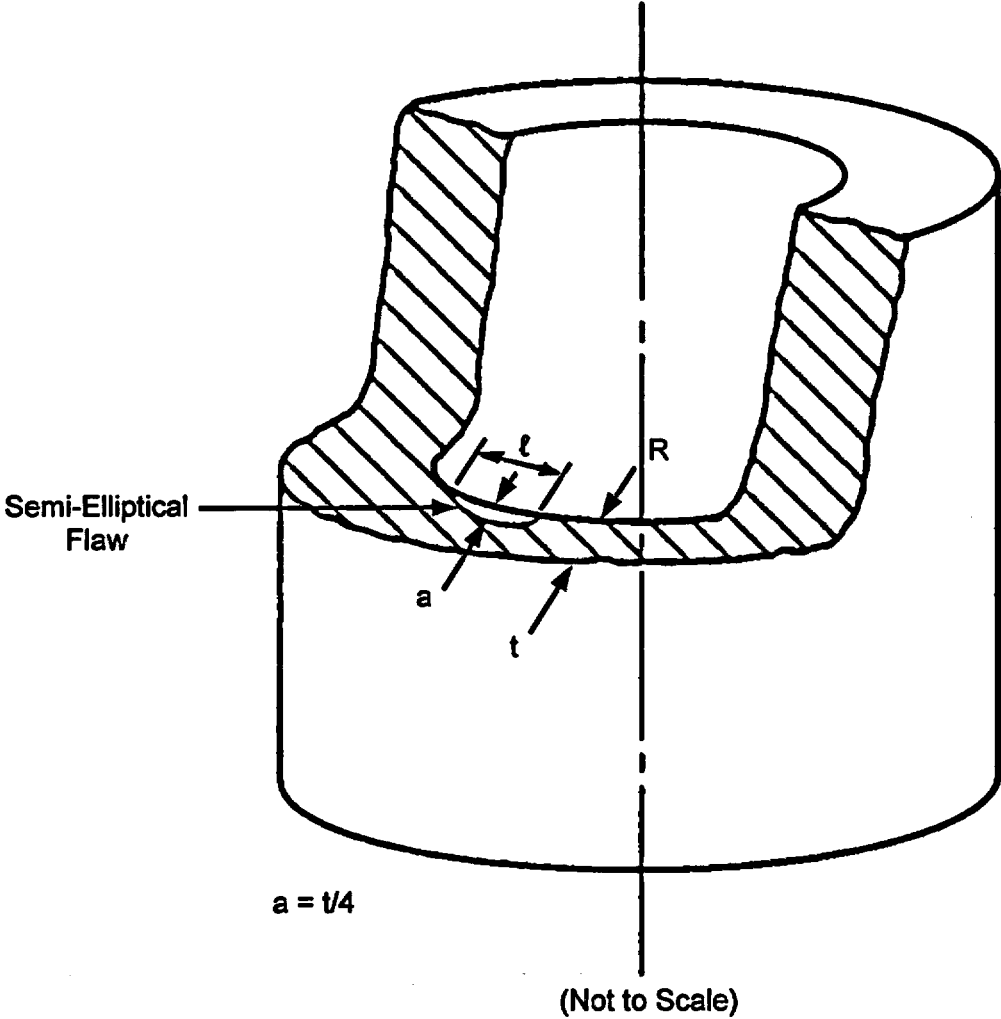


Figure 2-2 Reactor Vessel Beltline Region with Postulated Circumferential Flaw



### 3. Material Properties and Reactor Vessel Design Data

An upper-shelf fracture toughness material model is presented below, as well as mechanical properties for the weld material and reactor vessel design data.

#### 3.1 J-Integral Resistance Model for Mn-Mo-Ni/Linde 80 Welds

A model for the  $J$ -integral resistance versus crack extension curve ( $J$ - $R$  curve) required to analyze low upper-shelf energy materials has been derived specifically for Mn-Mo-Ni/Linde 80 weld materials. A previous analysis of the reactor vessels of B&W Owners Group RVWG [2] described the development of this toughness model from a large database of fracture specimens. Using a modified power law to represent the  $J$ - $R$  curve, the mean value of the  $J$ -integral is given by:

$$J = 1000 C_1 (\Delta a)^{C_2} \exp(C_3 \Delta a^{C_4})$$

with

$$\ln(C_1) = a_1 + a_2 Cu(\phi_t)^{a_7} + a_3 T + a_4 \ln(B_N)$$

$$C_2 = d_1 + d_2 \ln(C_1) + d_3 \ln(B_N)$$

$$C_3 = d_4 + d_5 \ln(C_1) + d_6 \ln(B_N)$$

$$C_4 = -0.4489$$

where

$\Delta a$  = crack extension, in.

$Cu$  = copper content, wt%

$\phi_t$  = fluence at crack tip,  $10^{18}$  n/cm<sup>2</sup>

$T$  = temperature, °F

$B_N$  = specimen net thickness, in.

and

$$a_1 = 1.81$$

$$a_2 = -1.512$$

$$a_3 = -0.00151$$

$$a_4 = 0.3935$$

$$a_7 = 0.1236$$

$$d_1 = 0.077$$

$$d_2 = 0.1164$$

$$d_3 = 0.07222$$

$$d_4 = -0.08124$$

$$d_5 = -0.00920$$

$$d_6 = 0.05183$$

A lower bound ( $-2S_e$ )  $J$ - $R$  curve is obtained by multiplying  $J$ -integrals from the mean  $J$ - $R$  curve by 0.699 [2]. It was shown in a previous low upper-shelf fracture toughness analysis performed for B&W Owners Group plants [3] that a typical lower bound  $J$ - $R$  curve is a conservative representation of toughness values for reactor vessel beltline materials, as required by Appendix K [1] for Levels A, B, and C Service Loadings. The best estimate representation of toughness required for Level D Service Loadings is provided by the mean  $J$ - $R$  curve.

### 3.2 Reactor Vessel Design Data

Pertinent design data for upper-shelf flaw evaluations in the beltline region of the reactor vessel are provided below for R. E. Ginna.

Design Pressure, $P_d$	= 2485 psig (use 2500 psig) [2]
Inside radius, $R_i$	= 66 in. [2]
Vessel thickness, $t$	= 6.5 in. [2]
Nominal cladding thickness, $t_c$	= 0.1875 in. [4]
Reactor coolant inlet temperature, $T_c$	= 528°F [5]

### 3.3 Mechanical Properties for Weld Material

The beltline region weld SA-847 has been previously determined [2] to be the limiting weld for the reactor vessel at R. E. Ginna. Mechanical properties for the base and weld materials are presented in Table 3-1.

Reactor vessel base metal:	SA-508, Grade 2, Class 1 low alloy steel forging [6] (changed from Class 2 to Grade 2, Class 1 in 1995)
Description:	3/4Ni-1/2Mo-1/3Cr-V [7]
Carbon content:	< 0.30% [6]
Linde 80 weld flux:	SA-847 [2]



Table 3-1 Mechanical Properties for Beltline Materials

Temp.	$E$	Yield Strength ( $\sigma_y$ )		Ultimate Strength ( $\sigma_u$ ) <sup>1</sup>		$\alpha$
Material:	Base Metal	Base Metal	Weld SA-847	Base Metal	Weld SA-847	Base Metal
Source: [Ref.]	Code [7]	Code [7]	Actual [8]	Code [7]	Actual [8]	Code [7]
(°F)	(ksi)	(ksi)	(ksi)	(ksi)	(ksi)	(in/in/°F)
100	27800	50.0	95.00	80.0	99.8	6.50E-06
200	27100	47.5	89.60	80.0	99.8	6.67E-06
300	26700	46.1	86.01	80.0	99.8	6.87E-06
400	26100	45.1	84.77	80.0	99.8	7.07E-06
500	25700	44.5	84.26	80.0	99.8	7.25E-06
528	25560	44.2	84.11	80.0	99.8	7.30E-06
600	25200	43.8	83.74	80.0	99.8	7.42E-06

Also, Poisson's ratio,  $\nu$ , is taken to be 0.3.

The ASME transition region fracture toughness curve for  $K_{Ic}$ , used to define the beginning of the upper-shelf toughness region, is indexed by the initial  $RT_{NDT}$  of the weld material. For SA-847,

$$\text{Initial } RT_{NDT} = -4.8^\circ\text{F} [9]$$

$$\text{Margin} = 48.3^\circ\text{F} [10]$$

### 3.4 J-Integral Resistance for SA-847 Weld Material

Values of J-integral resistance from the upper-shelf toughness model of Section 3.1 are dependent on the temperature and fluence at the crack tip location, the copper content of the weld material, and the size (thickness) of the fracture specimen. These parameters are listed below for the reactor vessel at R. E. Ginna.

$$\text{Projected inside surface fluence at 54 EFPY, } \phi_{t,IS} = 5.01 \times 10^{19} \text{ n/cm}^2 [9]$$

$$\text{Copper content of SA-847 weld material, } Cu = 0.25 \text{ wt\%} [10]$$

$$\text{Net specimen thickness, } B_N = 0.8 \text{ in.} [2]$$

<sup>1</sup> The ultimate strength values of the base and weld metals given here are not used in calculations

Crack tip temperature varies with plant operation. At 100% power normal operating conditions, the temperature at the crack tip,  $T$ , is taken to be the inlet temperature, or

$$\text{Crack tip temperature, } T = T_C = 528 \text{ }^\circ\text{F}$$

Fluence at the crack tip is determined using the attenuation equation from Regulatory Guide 1.99, Rev. 2 [11]:

$$\phi_t = \phi_{tIS} e^{-0.24x}$$

where

$\phi_t$  = attenuated fluence at crack tip, n/cm<sup>2</sup>

$\phi_{tIS}$  = fluence at inside surface, n/cm<sup>2</sup>

$x$  = depth into the vessel wall, in.

Values of the  $J$ -integral resistance at a ductile flaw extension of 0.10 in.,  $J_{0.1}$ , can then be defined for the following flaw depths:

Flaw Depth $a$ (in.)	Extension $\Delta a$ (in.)	Total Depth $x = a + \Delta a$ (in.)	Fluence $\phi_t$ ( $10^{18}$ n/cm <sup>2</sup> )	$J$ -Integral Resistance, $J_{0.1}$	
				Mean (lb/in)	Lower Bound (lb/in)
$t/4 = 1.625$	0.1	1.725	33.12	853	596
$t/10 = 0.650$	0.1	0.750	41.85	842	589

#### 4. Analytical Methodology

Upper-shelf toughness is evaluated through use of fracture mechanics analytical methods that utilize the acceptance criteria and evaluation procedures of Section XI, Appendix K [1], where applicable. Since the R. E. Ginna reactor vessel contains only circumferential welds in the beltline region, only circumferentially oriented flaws need be addressed in the present analysis.

##### 4.1 Procedure for Evaluating Levels A and B Service Loadings

The applied  $J$ -integral is calculated per Appendix K, paragraph K-4210 [1], using an effective flaw depth to account for small scale yielding at the crack tip, and evaluated per K-4220 for upper-shelf toughness and per K-4310 for flaw stability, as outlined below.

- (1) For a circumferential flaw of depth  $a$ , the stress intensity factor due to internal pressure is calculated with a safety factor ( $SF$ ) on pressure using the following:

$$K_{ip} = (SF)p \left( 1 + \frac{R_i}{2t} \right) (\pi a)^{0.5} F_2$$

where

$$F_2 = 0.885 + 0.233 \left( \frac{a}{t} \right) + 0.345 \left( \frac{a}{t} \right)^2, \quad 0.20 \leq \left( \frac{a}{t} \right) \leq 0.50$$

- (2) For a circumferential flaw of depth  $a$ , the stress intensity factor due to radial thermal gradients is calculated using the following:

$$K_{it} = C_m (CR) t^{2.5} F_3, \quad 0 \leq (CR) \leq 100 \text{ } ^\circ\text{F/hr}$$

where for SA-508, Class 2 steels the material coefficient  $C_m$  is defined in Appendix K [1] as:

$$C_m = \frac{E\alpha}{(1-\nu)d} = 0.0051,$$

$CR$  = cooldown rate ( $^\circ\text{F/hr}$ ), and

$$F_3 = 0.1181 + 0.5353 \left( \frac{a}{t} \right) - 1.273 \left( \frac{a}{t} \right)^2 + 0.6046 \left( \frac{a}{t} \right)^3, \quad 0.20 \leq \left( \frac{a}{t} \right) \leq 0.50$$

- (3) The effective flaw depth for small scale yielding,  $a_e$ , is calculated using the following:

$$a_e = a + \left( \frac{1}{6\pi} \right) \left[ \frac{K_{I_p} + K_{II}}{\sigma_y} \right]^2$$

- (4) For a circumferential flaw of depth  $a_e$ , the stress intensity factor due to internal pressure is

$$K'_{I_p} = (SF)\rho \left( 1 + \frac{R_I}{2t} \right) (\pi a_e)^{0.5} F'_2$$

where

$$F'_2 = 0.885 + 0.233 \left( \frac{a_e}{t} \right) + 0.345 \left( \frac{a_e}{t} \right)^2, \quad 0.20 \leq \left( \frac{a_e}{t} \right) \leq 0.50$$

- (5) For a circumferential flaw of depth  $a_e$ , the stress intensity factor due to radial thermal gradients is

$$K'_{II} = C_m (CR) t^{2.5} F'_3, \quad 0 \leq (CR) \leq 100 \text{ }^\circ\text{F/hr}$$

where

$$F'_3 = 0.1181 + 0.5353 \left( \frac{a_e}{t} \right) - 1.273 \left( \frac{a_e}{t} \right)^2 + 0.6046 \left( \frac{a_e}{t} \right)^3, \quad 0.20 \leq \left( \frac{a_e}{t} \right) \leq 0.50$$

- (6) The  $J$ -integral due to applied loads for small scale yielding is calculated using the following:

$$J_1 = 1000 \frac{(K'_{I_p} + K'_{II})^2}{E'}$$

where

$$E' = \frac{E}{1-\nu^2}$$

- (7) Evaluation of upper-shelf toughness at a flaw extension of 0.10 in. is performed for a flaw depth,

$$a = 0.25t + 0.10\text{in.},$$

using

$$SF = 1.15$$

$$p = P_s$$

where  $P_s$  is the accumulation pressure for Levels A and B Service Loadings, such that

$$J_1 < J_{0.1}$$

where

$J_1$  = the applied  $J$ -integral for a safety factor of 1.15 on pressure, and a safety factor of 1.0 on thermal loading

$J_{0.1}$  = the  $J$ -integral resistance at a ductile flaw extension of 0.10 in.

- (8) Evaluation of flaw stability is performed through use of a crack driving force diagram procedure by comparing the slopes of the applied  $J$ -integral curve and the  $J$ - $R$  curve. The applied  $J$ -integral is calculated for a series of flaw depths corresponding to increasing amounts of ductile flaw extension. The applied pressure is the accumulation pressure for Levels A and B Service Loadings,  $P_s$ , and the safety factor ( $SF$ ) on pressure is 1.25. Flaw stability at a given applied load is verified when the slope of the applied  $J$ -integral curve is less than the slope of the  $J$ - $R$  curve at the point on the  $J$ - $R$  curve where the two curves intersect.

#### 4.2 Procedure for Evaluating Levels C and D Service Loadings

Levels C and D Service Loadings are evaluated using the one-dimensional, finite element, thermal and stress models and linear elastic fracture mechanics methodology of the PCRIT computer code to determine stress intensity factors. The limiting transient for the R. E. Ginna vessel is discussed in BAW-2178 [4]. The Ginna Station is an older vintage plant; therefore its UFSAR did not present primary system analyses in terms of ASME service levels and service limits. As such, the available Ginna service levels C and D transients did not directly reflect worst-case fracture mechanics conditions. However, these transients appear to be bounded by the transients provided for other Westinghouse-designed plants. The analysis of Ref. [4] determined that for Level C loading conditions, the Turkey Point Steam Line Break without Offsite Power transient (TPSLB), which is a service level D transient, bounded all Level C transients for Westinghouse-designed plants. For Level D loading conditions, it was also determined that the TPSLB was the limiting transient. Therefore this transient will be used for the Levels C and D low upper-shelf fracture toughness analysis of the R. E. Ginna vessel.

The evaluation is performed as follows:

- (1) Utilize PCRT to calculate stress intensity factors for a semi-elliptical flaw of depth  $1/10$  of the base metal wall thickness, as a function of time, due to internal pressure and radial thermal gradients with a factor of safety of 1.0 on loading. The critical time in the transient occurs at that point where the stress intensity factor most closely approaches the upper-shelf toughness curve.
- (2) At the critical transient time, develop a crack driving force diagram with the applied  $J$ -integral and  $J$ - $R$  curves plotted as a function of flaw extension. The adequacy of the upper-shelf toughness is evaluated by comparing the applied  $J$ -integral with the  $J$ - $R$  curve at a flaw extension of 0.10 in. Flaw stability is assessed by examining the slopes of the applied  $J$ -integral and  $J$ - $R$  curves at the points of intersection.
- (3) Verify that the extent of stable flaw extension is no greater than 75% of the vessel wall thickness by determining when the applied  $J$ -integral curve intersects the mean  $J$ - $R$  curve.
- (4) Verify that the remaining ligament is not subject to tensile instability. The internal pressure  $p$  shall be less than  $P_i$ , where  $P_i$  is the internal pressure at tensile instability of the remaining ligament. For a circumferential flaw,  $P_i$  is given by [12]:

$$P_i = 1.07\sigma_o \left[ \frac{1 - (A_c/A)}{(R_i/(2R_m t)) + (A_c/A)} \right]$$

where

$$\sigma_o = \frac{\sigma_y + \sigma_u}{2}$$

$$A = t(\ell + t)$$

$$A_c = \frac{\pi a \ell}{4}$$

and

$\ell$  = surface length of crack, six times the depth,  $a$   
 $R_m$  = mean radius of vessel

This equation for  $P_i$  includes the effect of pressure on the flaw face. This equation is valid for internal pressures not exceeding the pressure at tensile instability caused by the applied hoop stress acting over the nominal wall thickness of the vessel. This validity limit on pressure  $P_i$  is

$$P_i \leq 1.07\sigma_o \left[ \frac{t}{R_i} \right]$$

### 4.3 Temperature Range for Upper-Shelf Fracture Toughness Evaluations

Upper-shelf fracture toughness is determined through use of Charpy V-notch impact energy versus temperature plots by noting the temperature above which the Charpy energy remains on a plateau, maintaining a relatively high constant energy level. Similarly, fracture toughness can be addressed in three different regions on the temperature scale, i.e. a lower-shelf toughness region, a transition region, and an upper-shelf toughness region. Fracture toughness of reactor vessel steel and associated weld metals are conservatively predicted by the ASME initiation toughness curve,  $K_{Ic}$ , in lower-shelf and transition regions. In the upper-shelf region, the upper-shelf toughness curve,  $K_{Jc}$ , is derived from the upper-shelf  $J$ -integral resistance model described in Section 3.1. The upper-shelf toughness then becomes a function of fluence, copper content, temperature, and fracture specimen size. When upper-shelf toughness is plotted versus temperature, a plateau-like curve develops that decreases slightly with increasing temperature. Since the present analysis addresses the low upper-shelf fracture toughness issue, only the upper-shelf temperature range, which begins at the intersection of  $K_{Ic}$  and the upper-shelf toughness curves,  $K_{Jc}$ , is considered.

### 4.4 Effect of Cladding Material

The PCRIT code utilized in the flaw evaluations for Levels C and D Service Loadings does not consider stresses in the cladding when calculating stress intensity factors for thermal loads. To account for this cladding effect, an additional stress intensity factor,  $K_{Iclad}$ , is calculated separately and added to the total stress intensity factor computed by PCRIT.

The contribution of cladding stresses to stress intensity factor was examined previously [4]. In this low upper-shelf fracture toughness analysis performed for B&W Owners Group Reactor Vessel Working Group plants, it was shown that the limiting weld was the Zion-1 WF-70 weld and the limiting transient was the Turkey Point Steam Line Break without Offsite Power. The Zion vessel had the highest projected fluence and was as thick or thicker than any other vessel. The thicknesses of the reactor vessels for R. E. Ginna and Zion are 6.5" and 8.44", respectively. The nominal cladding thickness is 3/16" for both vessels. From a thermal stress perspective, it is conservative to consider the thicker vessel. For the Zion vessel, the maximum value of  $K_{Iclad}$ , at any time during the transient and for any flaw depth, was determined to be 9.0 ksi/in. This bounding value is therefore used as the stress intensity factor for  $K_{Iclad}$  in this R. E. Ginna low upper-shelf fracture toughness analysis.

## **5. Applied Loads**

The Levels A and B Service Loadings required by Appendix K are an accumulation pressure (internal pressure load) and a cooldown rate (thermal load). Since Levels C and D Service Loadings are not specified by the Code, Levels C and D pressurized thermal shock events are reviewed and a worst case transient is selected for use in flaw evaluations.

### **5.1 Levels A and B Service Loadings**

Per paragraph K-1300 of Appendix K [1], the accumulation pressure used for flaw evaluations should not exceed 1.1 times the design pressure. Using 2.5 ksi as the design pressure, the accumulation pressure is 2.75 ksi. The cooldown rate is also taken to be the maximum required by Appendix K, 100 °F/hour.

### **5.2 Levels C and D Service Loadings**

As discussed in Section 4.2, the conservative Turkey Point Steam Line Break without Offsite Power transient (TPSLB) is used for the PCRIT analysis of Levels C and D service loadings. Pressure and temperature time histories for this transient are shown in Figure 5-1. The PCRIT analysis of this transient was of sufficient duration to capture the peak value of stress intensity factor over time.



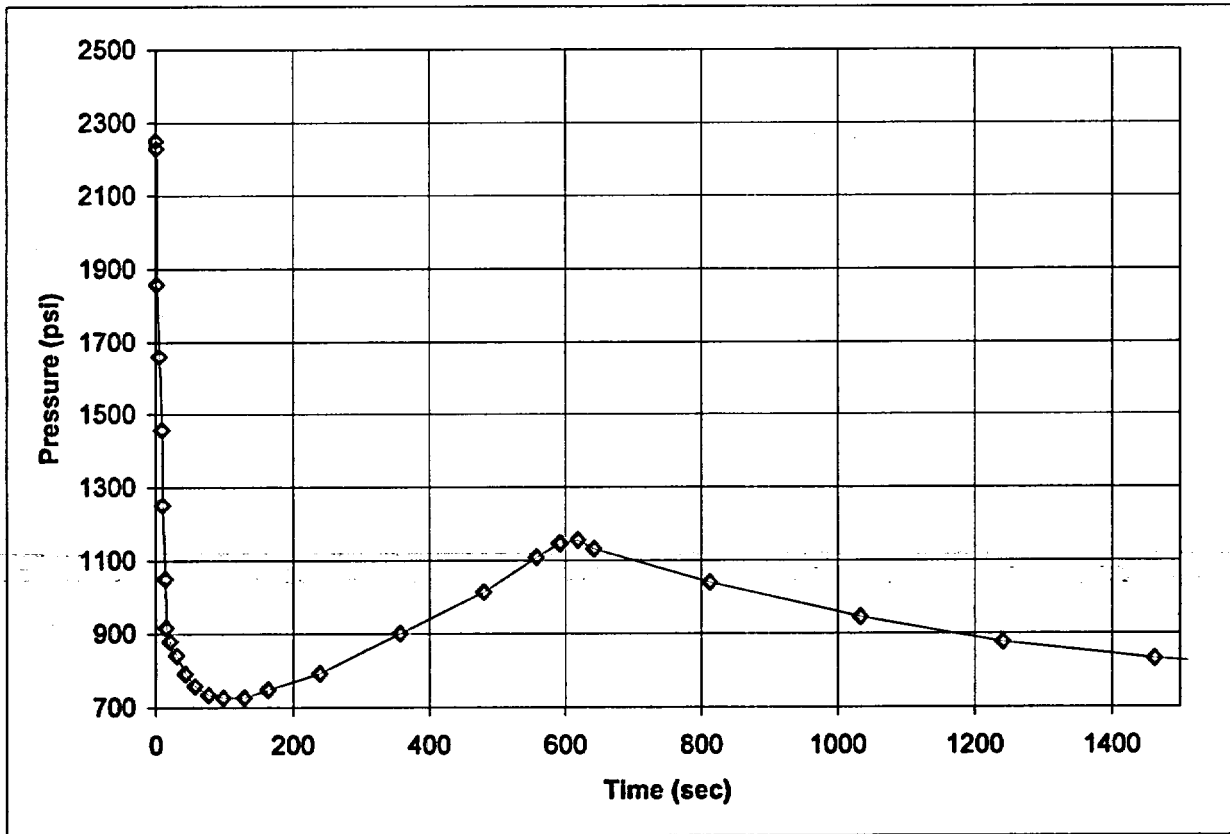
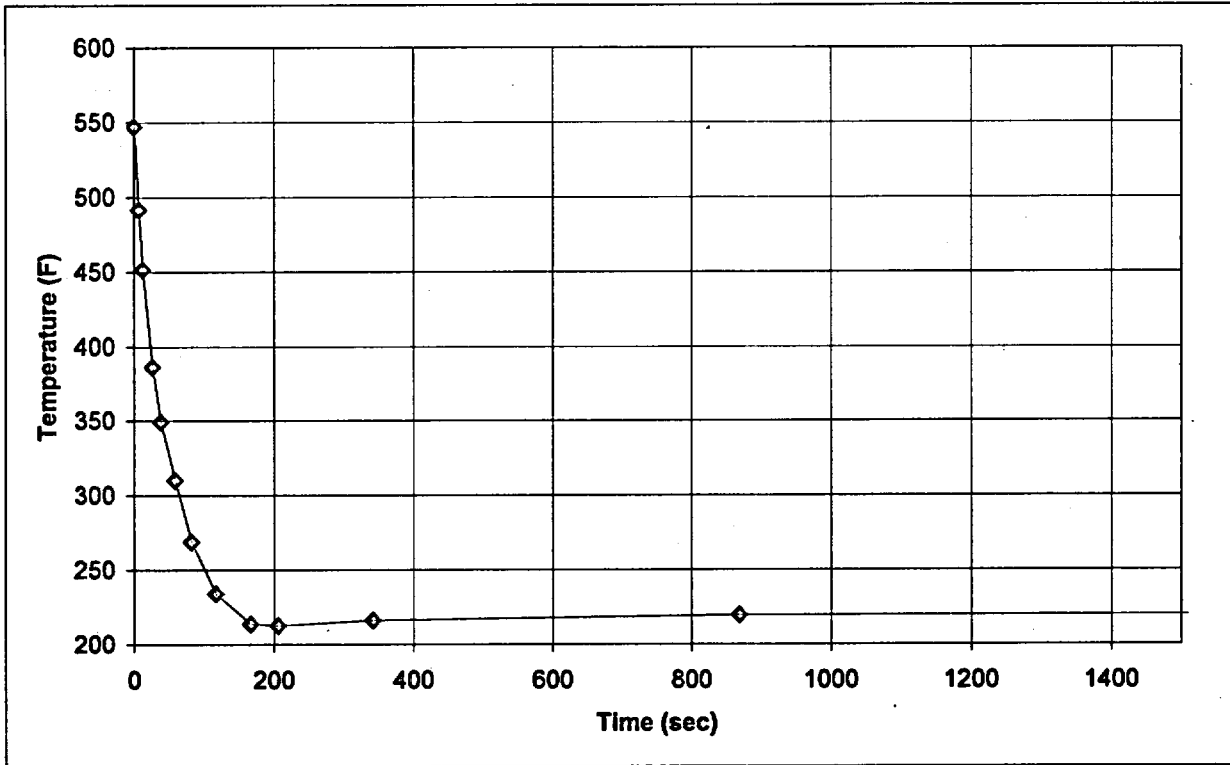


Figure 5-1 Steam Line Break without Offsite Power transient (TPSLB)

## 6. Evaluation for Levels A and B Service Loadings

Initial flaw depths equal to  $\frac{1}{4}$  of the vessel wall thickness are analyzed for Levels A and B Service Loadings following the procedure outlined in Section 4.1 and evaluated for acceptance based on values for the  $J$ -integral resistance of the material from Section 3.4. The results of the evaluation are presented in Table 6-1, where it is seen that the minimum ratio of material  $J$ -integral resistance ( $J_{0.1}$ ) to applied  $J$ -integral ( $J_1$ ) is 5.79 which is significantly higher than the minimum acceptable value of 1.0.

The flaw evaluation for the controlling weld (SA-847) is repeated by calculating applied  $J$ -integrals for various amounts of flaw extension with safety factors (on pressure) of 1.15 and 1.25 in Table 6-2. The results, along with mean and lower bound  $J$ - $R$  curves developed in Table 6-3, are plotted in Figure 6-1. An evaluation line at a flaw extension 0.10 in. is also included to confirm the results of Table 6-1 by showing that the applied  $J$ -integral for a safety factor of 1.15 is less than the lower bound  $J$ -integral resistance of the material. The requirement for ductile and stable crack growth is also demonstrated by Figure 6-1 since the slope of the applied  $J$ -integral curve for a safety factor of 1.25 is considerably less than the slope of the lower bound  $J$ - $R$  curve at the point where the two curves intersect.

Table 6-1 Flaw Evaluation for Levels A & B Service Loadings

Dimensional data:

$R_1 = 66$  in.  
 $t = 6.5$  in.  
 $a_o = 1.6250$  in.  
 $\Delta a = 0.1000$  in.  
 $a = 1.7250$  in.  
 $a/t = 0.2654$  ( $0.2 \leq a/t \leq 0.5$ )

Material data:

$T = 528$  F  
 $E = 25560$  ksi  
 $\nu = 0.3$   
 $E' = 28088$  ksi

Loading data:

$P_d = 2.50$  ksi  
 $P_s = 2.75$  ksi  
 $SF = 1.15$   
 $CR = 100$  F/hr

Geometry factors for initial flaw depth (w/o plasticity correction):

$F_1 = 1.0529$  for pressure loading and axial flaws  
 $F_2 = 0.9711$  for pressure loading and circumferential flaws  
 $F_3 = 0.1818$  for thermal loading and both flaw types  
 $C_m = 0.0051$  (ksi-hr)/(in<sup>2</sup>-°F)

Weld	Orient.	$K_{ip}$ (ksi/in)	$K_R$ (ksi/in)	$\sigma_y$ (ksi)	$a_o$ (in.)	$a_o/t$	$F_1'$ or $F_2'$	$F_3'$	$K_{ip}'$ (ksi/in)	$K_R'$ (ksi/in)	$J_1$ (lb/in)	$J_{0.1}$ at $1/4$ (lb/in)	$J_{0.1}/J_1$
SA-847	C	43.45	9.99	84.11	1.7464	0.2687	0.9725	0.1818	43.78	9.98	103	596	<b>5.79</b>

Table 6-2 J-Integral versus Flaw Extension for Levels A & B Service Loadings

$R_1 = 66$  in.  
 $t = 6.5$  in.  
 $a_o = 1.6250$  in.

$P_a = 2.75$  ksi  
 $CR = 100$  F/hr  
 $C_m = 0.0051$  (ksi-hr)/(in<sup>2</sup>-°F)  
 $\sigma_y = 84.11$  ksi

$\Delta a$ (in.)	a (in.)	SF = 1.15						SF = 1.25					
		$K_{I_p}$ (ksi/in)	$K_t$ (ksi/in)	$a_o$ (in.)	$K_{I_p}'$ (ksi/in)	$K_{I_t}'$ (ksi/in)	$J_1$ (lb/in)	$K_{I_p}$ (ksi/in)	$K_t$ (ksi/in)	$a_o$ (in.)	$K_{I_p}'$ (ksi/in)	$K_{I_t}'$ (ksi/in)	$J_1$ (lb/in)
0.000	1.625	41.89	9.99	1.6452	42.21	9.99	97	45.54	9.99	1.6481	45.93	9.99	111
0.025	1.65	42.28	9.99	1.6705	42.60	9.99	98	45.96	9.99	1.6735	46.36	9.99	113
0.050	1.675	42.67	9.99	1.6958	43.00	9.99	100	46.38	9.99	1.6988	46.79	9.99	115
0.075	1.7	43.06	9.99	1.7211	43.39	9.99	101	46.80	9.99	1.7242	47.21	9.99	116
0.100	1.725	43.45	9.99	1.7464	43.78	9.98	103	47.23	9.99	1.7495	47.64	9.98	118
0.125	1.75	43.83	9.98	1.7717	44.17	9.98	104	47.64	9.98	1.7749	48.06	9.98	120
0.150	1.775	44.22	9.98	1.7970	44.56	9.97	106	48.06	9.98	1.8003	48.49	9.97	122
0.175	1.8	44.60	9.97	1.8223	44.95	9.97	107	48.48	9.97	1.8256	48.91	9.97	123
0.200	1.825	44.99	9.97	1.8476	45.33	9.96	109	48.90	9.97	1.8510	49.33	9.96	125
0.225	1.85	45.37	9.96	1.8730	45.72	9.95	110	49.32	9.96	1.8763	49.75	9.95	127
0.250	1.875	45.75	9.95	1.8983	46.11	9.94	112	49.73	9.95	1.9017	50.18	9.94	129
0.275	1.9	46.14	9.94	1.9236	46.50	9.93	113	50.15	9.94	1.9271	50.60	9.92	130
0.300	1.925	46.52	9.93	1.9489	46.88	9.91	115	50.56	9.93	1.9524	51.02	9.91	132
0.325	1.95	46.90	9.91	1.9742	47.27	9.90	116	50.98	9.91	1.9778	51.44	9.90	134
0.350	1.975	47.28	9.90	1.9995	47.65	9.88	118	51.39	9.90	2.0032	51.86	9.88	136
0.375	2	47.66	9.88	2.0248	48.04	9.87	119	51.80	9.88	2.0285	52.28	9.86	137
0.400	2.025	48.04	9.87	2.0501	48.42	9.85	121	52.22	9.87	2.0539	52.70	9.85	139
0.425	2.05	48.42	9.85	2.0755	48.81	9.83	122	52.63	9.85	2.0793	53.11	9.83	141
0.450	2.075	48.80	9.83	2.1008	49.19	9.81	124	53.04	9.83	2.1046	53.53	9.81	143
0.475	2.1	49.18	9.81	2.1261	49.58	9.79	125	53.46	9.81	2.1300	53.95	9.78	145
0.500	2.125	49.56	9.79	2.1514	49.96	9.76	127	53.87	9.79	2.1554	54.37	9.76	146

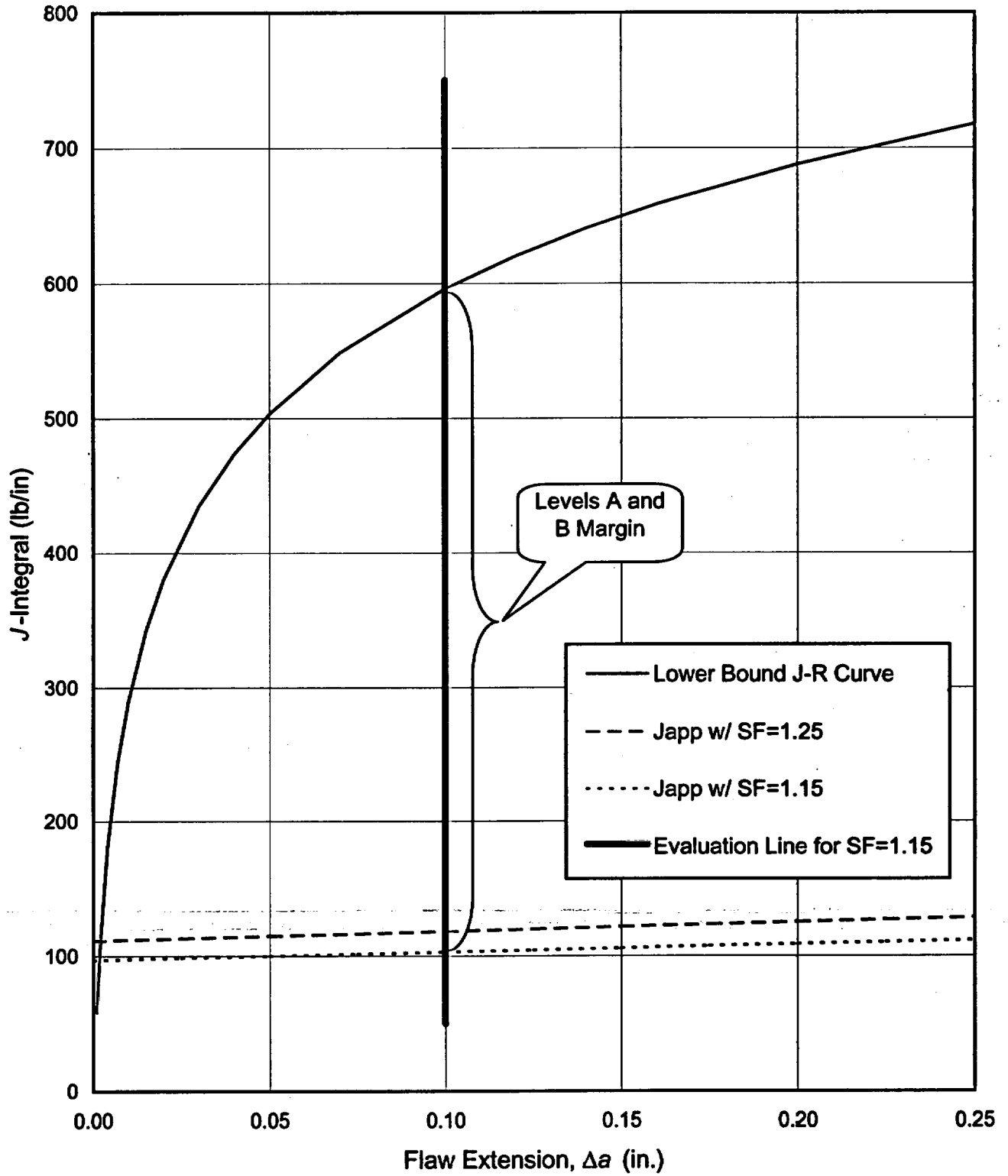
Table 6-3 J-R Curves for Evaluation of Levels A and B Service Loadings

Plant: R. E. GINNA

T = 528 F  
 t = 6.5 in.  
 a<sub>o</sub> = 1.625 in.  
 φ<sub>1s</sub> = 50.10 10<sup>18</sup> n/cm<sup>2</sup> @ inside surface  
 Cu = 0.25  
 B<sub>n</sub> = 0.80 in

Δa (in.)	a (in.)	φ <sub>1</sub> (10 <sup>18</sup> n/cm <sup>2</sup> )	ln C <sub>1</sub>	C <sub>1</sub>	C <sub>2</sub>	C <sub>3</sub>	J-R (lb/in)	
							Mean	Low
0.001	1.6260	33.9124	0.34060	1.40579	0.10053	-0.09594	83	58
0.002	1.6270	33.9043	0.34062	1.40582	0.10053	-0.09594	158	110
0.004	1.6290	33.8880	0.34065	1.40587	0.10054	-0.09594	257	180
0.007	1.6320	33.8636	0.34071	1.40594	0.10054	-0.09594	351	245
0.010	1.6350	33.8392	0.34076	1.40601	0.10055	-0.09594	415	290
0.015	1.6400	33.7987	0.34084	1.40613	0.10056	-0.09594	490	342
0.020	1.6450	33.7581	0.34093	1.40626	0.10057	-0.09594	544	381
0.030	1.6550	33.6772	0.34110	1.40650	0.10059	-0.09594	622	435
0.040	1.6650	33.5965	0.34128	1.40674	0.10061	-0.09594	677	474
0.050	1.6750	33.5159	0.34145	1.40699	0.10063	-0.09594	720	503
0.070	1.6950	33.3554	0.34180	1.40747	0.10067	-0.09595	785	549
0.100	1.7250	33.1161	0.34232	1.40820	0.10073	-0.09595	853	596
0.120	1.7450	32.9576	0.34266	1.40869	0.10077	-0.09595	887	620
0.140	1.7650	32.7998	0.34301	1.40918	0.10081	-0.09596	917	641
0.160	1.7850	32.6427	0.34335	1.40966	0.10085	-0.09596	942	658
0.200	1.8250	32.3308	0.34404	1.41064	0.10093	-0.09597	984	688
0.250	1.8750	31.9452	0.34490	1.41185	0.10103	-0.09598	1026	718
0.300	1.9250	31.5641	0.34576	1.41307	0.10113	-0.09598	1061	742
0.350	1.9750	31.1876	0.34662	1.41428	0.10123	-0.09599	1090	762
0.400	2.0250	30.8156	0.34748	1.41549	0.10133	-0.09600	1116	780
0.450	2.0750	30.4480	0.34833	1.41670	0.10143	-0.09601	1139	796
0.500	2.1250	30.0848	0.34919	1.41791	0.10153	-0.09601	1159	810

Figure 6-1 J-Integral vs. Flaw Extension for Levels A & B Service Loadings



## 7. Evaluation for Levels C and D Service Loadings

A flaw depth of  $1/10$  of the base metal wall thickness is used to evaluate the Levels C and D Service Loadings. Table 7-1 presents applied stress intensity factors,  $K_I$ , from the PCRIT pressurized thermal shock analysis of the steam line break transient described in Section 5.2, along with total stress intensity factors after including a contribution of 9.0 ksi√in from cladding, as discussed in Section 4.4. The stress intensity factor calculated by the PCRIT code is the sum of thermal, residual stress, deadweight, and pressure terms. Table 7-1 also shows the variation of crack tip temperature with time for the TPSLB event. To determine the critical time in the transient for the Levels C and D flaw evaluation, allowable stress intensity factors are calculated for both the transition and upper-shelf toughness regions. Transition region toughness is obtained from the ASME Section XI equation for crack initiation [13],

$$K_{Ic} = 33.2 + 2.806 \exp[0.02(T - RT_{NDT} + 100^\circ\text{F})]$$

using an  $RT_{NDT}$  value of 277.1°F from PCRIT for a flaw depth of  $1/10$  of the wall thickness, where:

$$\begin{aligned} K_{Ic} &= \text{transition region toughness, ksi}\sqrt{\text{in}} \\ T &= \text{crack tip temperature, }^\circ\text{F} \end{aligned}$$

Upper-shelf toughness is derived from the  $J$ -integral resistance model of Section 3.1 for a flaw depth of  $1/10$  of the wall thickness, a crack extension of 0.10 in., and a fluence value of  $41.85 \times 10^{18}$  n/cm<sup>2</sup>, as follows:

$$K_{Jc} = \sqrt{\frac{J_{0.1}E}{1000(1-\nu^2)}}$$

where

$$\begin{aligned} K_{Jc} &= \text{upper-shelf region toughness, ksi}\sqrt{\text{in}} \\ J_{0.1} &= J\text{-integral resistance at } \Delta a = 0.1 \text{ in.} \end{aligned}$$

Toughness values are given in Tables 7-2 and 7-3 for the transition and upper-shelf regions, respectively, as a function of temperature.

Figure 7-1 shows the variation of applied stress intensity factor,  $K_I$ , transition range toughness,  $K_{Ic}$ , and upper-shelf toughness,  $K_{Jc}$  with temperature. The small triangles on the  $K_I$  curve indicate points in time at which PCRIT solutions are available. In the upper-shelf toughness range, the  $K_I$  curve is closest to the lower bound  $K_{Jc}$  curve at 3.6 minutes into the transient. This time is selected as the critical time in the transient at which to perform the flaw evaluation for Levels C and D Service Loadings.

Applied  $J$ -integrals are calculated for the controlling weld (SA-847) for various flaw depths in Table 7-4 using stress intensity factors from PCRIT for the steam line break transient (at 3.6 min.) and adding 9.0 ksi√in to account for cladding effects. Stress intensity factors are converted to  $J$ -integrals by the plain strain relationship,

$$J_{\text{applied}}(a) = 1000 \frac{K_{I\text{total}}^2(a)}{E} (1-\nu^2)$$

Table 7-4 lists flaw extensions vs. applied  $J$ -integrals. As the Ginna vessel is 6.5 in. thick, the initial flaw depth of  $1/10$  of the wall thickness is 0.65 in. Flaw extension from this flaw depth is calculated by subtracting 0.65 in. from the built-in PCRIT flaw depths. The results, along with mean and lower bound  $J$ - $R$  curves developed in Table 7-5, are plotted in Figure 7-2. An evaluation line is used at a flaw extension 0.10 in. to show that the applied  $J$ -integral is less than the lower bound  $J$ -integral of the material, as required by Appendix K [1]. The requirements for ductile and stable crack growth are also demonstrated by Figure 7-2 since the slope of the applied  $J$ -integral curve is considerably less than the slopes of both the lower bound and mean  $J$ - $R$  curves at the points of intersection.

Referring to Figure 7-2, the Level D Service Loading requirement that the extent of stable flaw extension be no greater than 75% of the vessel wall thickness is easily satisfied since the applied  $J$ -integral curve intersects the mean  $J$ - $R$  curve at a flaw extension that is only a small fraction of the wall thickness (less than 1%).

The last requirement is that the internal pressure  $p$  shall be less than  $P_i$ , the internal pressure at tensile instability of the remaining ligament. Table 7-6 gives the results of the calculations for  $P_i$  for flaw depths up to 1.04 in. The calculated validity limit of  $P_i$  is 9.69 ksi. The calculated values of  $P_i$  shown in Table 7-1 exceed this validity limit for all flaw depths of concern. The internal pressure  $p$  is much less than the validity limit of  $P_i$ ; therefore the remaining ligament is not subject to tensile instability.



Table 7-1  $K_I$  vs. Crack Tip Temperature for TP SLB

a/t = 1/10 a = 0.650 in.				
Time	Temp	PCRIT $K_{Isum}$	Clad $K_I$	Total $K_I$
0.00	547.00	29.31	9.0	38.31
0.10	546.90	25.21	9.0	34.21
0.20	545.50	23.65	9.0	32.65
0.30	541.70	24.42	9.0	33.42
0.40	536.20	27.16	9.0	36.16
0.50	529.40	30.07	9.0	39.07
0.60	521.90	32.87	9.0	41.87
0.70	514.10	35.55	9.0	44.55
0.80	506.20	38.04	9.0	47.04
0.90	498.40	40.37	9.0	49.37
1.00	490.80	42.59	9.0	51.59
1.10	483.40	44.75	9.0	53.75
1.20	476.10	46.82	9.0	55.82
1.30	469.00	48.83	9.0	57.83
1.40	462.10	50.83	9.0	59.83
1.50	455.20	52.70	9.0	61.70
1.60	448.50	54.40	9.0	63.40
1.70	442.20	56.00	9.0	65.00
1.80	436.00	57.53	9.0	66.53
1.90	430.10	59.00	9.0	68.00
2.00	424.40	60.40	9.0	69.40
2.10	418.80	61.65	9.0	70.65
2.20	413.60	62.79	9.0	71.79
2.30	408.60	63.85	9.0	72.85
2.40	403.90	64.83	9.0	73.83
2.50	399.40	65.74	9.0	74.74
2.60	395.10	66.61	9.0	75.61
2.70	391.00	67.43	9.0	76.43
2.80	387.10	68.21	9.0	77.21
2.90	383.30	68.91	9.0	77.91
3.00	379.70	69.51	9.0	78.51
3.10	376.40	70.02	9.0	79.02
3.20	373.20	70.48	9.0	79.48
3.30	370.30	70.89	9.0	79.89
3.40	367.50	71.25	9.0	80.25
3.50	364.90	71.57	9.0	80.57
3.60	362.40	71.85	9.0	80.85
3.80	357.90	72.30	9.0	81.30
4.00	353.80	72.63	9.0	81.63

Table 7-1  $K_I$  vs. Crack Tip Temperature for TPSLB (continued)

a/t = 1/10 a = 0.650 in.				
Time	Temp	PCRIT $K_{Isum}$	Clad $K_I$	Total $K_I$
4.20	350.10	72.91	9.0	81.91
4.40	346.70	73.10	9.0	82.10
4.60	343.60	73.24	9.0	82.24
4.80	340.80	73.32	9.0	82.32
5.00	338.20	73.35	9.0	82.35
5.20	335.80	73.34	9.0	82.34
5.40	333.50	73.29	9.0	82.29
5.60	331.40	73.22	9.0	82.22
5.80	329.40	73.12	9.0	82.12
6.00	327.50	73.01	9.0	82.01
6.20	325.80	72.88	9.0	81.88
6.40	324.10	72.74	9.0	81.74
6.60	322.40	72.59	9.0	81.59
6.80	320.90	72.42	9.0	81.42
7.00	319.40	72.25	9.0	81.25
7.20	318.00	72.06	9.0	81.06
7.40	316.70	71.86	9.0	80.86
7.60	315.40	71.66	9.0	80.66
7.80	314.10	71.45	9.0	80.45
8.00	312.90	71.23	9.0	80.23
8.20	311.80	71.04	9.0	80.04
8.40	310.70	70.84	9.0	79.84
8.70	309.10	70.53	9.0	79.53
9.00	307.60	70.22	9.0	79.22
9.50	305.20	69.67	9.0	78.67
10.00	303.10	69.04	9.0	78.04
10.50	301.00	68.16	9.0	77.16
11.00	299.10	67.13	9.0	76.13
12.00	295.70	65.17	9.0	74.17
14.00	289.70	61.36	9.0	70.36
16.00	284.50	57.86	9.0	66.86
19.00	277.40	53.14	9.0	62.14
22.00	271.20	49.02	9.0	58.02
25.01	265.70	45.44	9.0	54.44
29.01	259.70	41.24	9.0	50.24
33.35	255.00	37.34	9.0	46.34

Table 7-2  $K_{Ic}$  at 1/10 Wall Thickness

K <sub>Ic</sub> Curve at a = 1/10T		
RT <sub>NDT</sub> = 277.1 F		
T (F)	T-RT <sub>NDT</sub>	K <sub>Ic</sub> (ksi√in)
200	-77.1	37.6
210	-67.1	38.6
220	-57.1	39.8
230	-47.1	41.3
240	-37.1	43.1
250	-27.1	45.3
260	-17.1	47.9
270	-7.1	51.2
280	2.9	55.2
290	12.9	60.0
300	22.9	66.0
310	32.9	73.2
320	42.9	82.1
330	52.9	92.9
340	62.9	106.2
350	72.9	122.3
360	82.9	142.0
370	92.9	166.1
380	102.9	195.6
390	112.9	231.5
400	122.9	275.4
410	132.9	329.0
420	142.9	394.5
430	152.9	474.5
440	162.9	572.2
450	172.9	691.6

Table 7-3  $K_{Jc}$  at 1/10 Wall Thickness with  $\Delta a = 0.10$  in.

K <sub>Jc</sub> Curve with $\Delta a = 0.10$ in.								
Fluence = 50.10 x 10 <sup>18</sup> n/cm <sup>2</sup> at inside surface = 41.85 x 10 <sup>18</sup> n/cm <sup>2</sup> at t/10 + 0.1"								
$\Delta a = 0.10$ in. Cu = 0.25 Wt-% E = 25560 ksi $\nu = 0.30$ C <sub>4</sub> = -0.4489								
T (F)	lnC <sub>1</sub>	C <sub>1</sub>	C <sub>2</sub>	C <sub>3</sub>	Mean J <sub>0.1</sub> (lb/in)	Lower Bound J <sub>0.1</sub> (lb/in)	Mean K <sub>Jc</sub> (ksiv/in)	Lower Bound K <sub>Jc</sub> (ksiv/in)
200	0.82050	2.27163	0.15639	-0.10035	1195	836	183.2	153.2
250	0.74500	2.10644	0.14760	-0.09965	1133	792	178.4	149.2
300	0.66950	1.95326	0.13881	-0.09896	1074	751	173.7	145.2
350	0.59400	1.81122	0.13003	-0.09826	1019	712	169.1	141.4
400	0.51850	1.67951	0.12124	-0.09757	966	675	164.7	137.7
450	0.44300	1.55737	0.11245	-0.09688	916	640	160.4	134.1
500	0.36750	1.44412	0.10366	-0.09618	868	607	156.1	130.5
550	0.29200	1.33910	0.09487	-0.09549	823	575	152.0	127.1
600	0.21650	1.24172	0.08609	-0.09480	780	545	148.0	123.8

Table 7-4 J-Integral vs. Flaw Extension for Levels C and D Service Loadings

Time = 3.60 min.		t = 6.5 in.		E = 25560 ksi		v = 0.3	
Crack tip at t/10		t = 6.5 in.		E = 25560 ksi		v = 0.3	
(a/t)*40	a (in.)	$\Delta a$ (in.)	Temp. (F)	$K_{Isum}$	$K_{Iclad}$	$K_{Itotal}$	$J_{app}$ (lb/in)
1	0.1625		308.60	43.50	9.0	52.5	98
2	0.3250		327.20	59.20	9.0	68.2	166
3	0.4875		345.20	67.13	9.0	76.1	206
4	0.6500	0.0000	362.40	71.85	9.0	80.9	233
5	0.8125	0.1625	378.80	74.70	9.0	83.7	249
6	0.9750	0.3250	394.30	76.30	9.0	85.3	259
7	1.1375	0.4875	409.00	76.94	9.0	85.9	263
8	1.3000	0.6500	422.70	77.00	9.0	86.0	263
9	1.4625	0.8125	435.50	76.38	9.0	85.4	260
10	1.6250	0.9750	447.30	75.54	9.0	84.5	254
12	1.9500	1.3000	468.30	72.84	9.0	81.8	238
14	2.2750	1.6250	485.80	69.35	9.0	78.4	219
16	2.6000	1.9500	500.10	65.66	9.0	74.7	198
18	2.9250	2.2750	511.60	61.35	9.0	70.4	176
20	3.2500	2.6000	520.70	56.66	9.0	65.7	153
22	3.5750	2.9250	527.80	52.02	9.0	61.0	133
24	3.9000	3.2500	533.10	47.23	9.0	56.2	113
26	4.2250	3.5750	537.20	42.82	9.0	51.8	96
28	4.5500	3.9000	540.10	38.97	9.0	48.0	82
30	4.8750	4.2250	542.20	35.67	9.0	44.7	71
32	5.2000	4.5500	543.70	32.64	9.0	41.6	62

Note: At  $\Delta a = 0.10$  in.,  $J_{app} = 243$  lb/in.

Table 7-5 J-R Curves for Evaluation of Levels C and D Service Loadings

Plant: R. E. GINNA

Time = 3.60 min.  
 T = 362.4 F  
 t = 6.5 in.  
 a<sub>o</sub> = 0.65 in.  
 φ<sub>IS</sub> = 50.10 10<sup>18</sup> n/cm<sup>2</sup> @ inside surface  
 Cu = 0.25  
 B<sub>n</sub> = 0.80 in

Δa (in.)	a (in.)	φ <sub>t</sub> (10 <sup>18</sup> n/cm <sup>2</sup> )	ln C <sub>1</sub>	C <sub>1</sub>	C <sub>2</sub>	C <sub>3</sub>	J-R (lb/in)	
							Mean	Low
0.001	0.6510	42.8532	0.57351	1.77449	0.12764	-0.09808	83	58
0.002	0.6520	42.8429	0.57353	1.77452	0.12764	-0.09808	163	114
0.004	0.6540	42.8224	0.57357	1.77458	0.12765	-0.09808	272	190
0.007	0.6570	42.7916	0.57362	1.77468	0.12765	-0.09808	379	265
0.010	0.6600	42.7608	0.57367	1.77477	0.12766	-0.09808	454	317
0.015	0.6650	42.7095	0.57376	1.77493	0.12767	-0.09808	544	380
0.020	0.6700	42.6583	0.57385	1.77509	0.12768	-0.09808	610	427
0.030	0.6800	42.5560	0.57403	1.77541	0.12770	-0.09808	707	494
0.040	0.6900	42.4540	0.57421	1.77572	0.12772	-0.09808	777	543
0.050	0.7000	42.3522	0.57439	1.77604	0.12774	-0.09808	831	581
0.070	0.7200	42.1494	0.57474	1.77667	0.12778	-0.09809	915	640
0.100	0.7500	41.8470	0.57528	1.77762	0.12785	-0.09809	1005	703
0.120	0.7700	41.6467	0.57563	1.77825	0.12789	-0.09810	1052	735
0.140	0.7900	41.4472	0.57599	1.77888	0.12793	-0.09810	1091	763
0.160	0.8100	41.2488	0.57634	1.77952	0.12797	-0.09810	1126	787
0.200	0.8500	40.8547	0.57705	1.78078	0.12805	-0.09811	1184	828
0.250	0.9000	40.3673	0.57794	1.78236	0.12816	-0.09812	1243	869
0.300	0.9500	39.8858	0.57882	1.78394	0.12826	-0.09812	1292	903
0.350	1.0000	39.4101	0.57971	1.78551	0.12836	-0.09813	1333	932
0.400	1.0500	38.9400	0.58059	1.78709	0.12847	-0.09814	1370	958
0.450	1.1000	38.4755	0.58147	1.78866	0.12857	-0.09815	1403	981
0.500	1.1500	38.0165	0.58235	1.79024	0.12867	-0.09816	1432	1001

**Table 7.6 Level D Service Loadings - Internal Pressure at Tensile Instability**

<b>flaw depth <math>a</math> (in.)</b>	<b><math>P_t</math> (ksi)</b>
0.065	20.32
0.130	20.29
0.195	20.25
0.260	20.19
0.325	20.11
0.390	20.03
0.455	19.94
0.520	19.84
0.585	19.73
0.650	19.62
0.715	19.50
0.780	19.37
0.845	19.25
0.910	19.12
0.975	18.98
1.040	18.84

Figure 7-1  $K_I$  vs. Crack Tip Temperature for Levels C & D Service Loadings

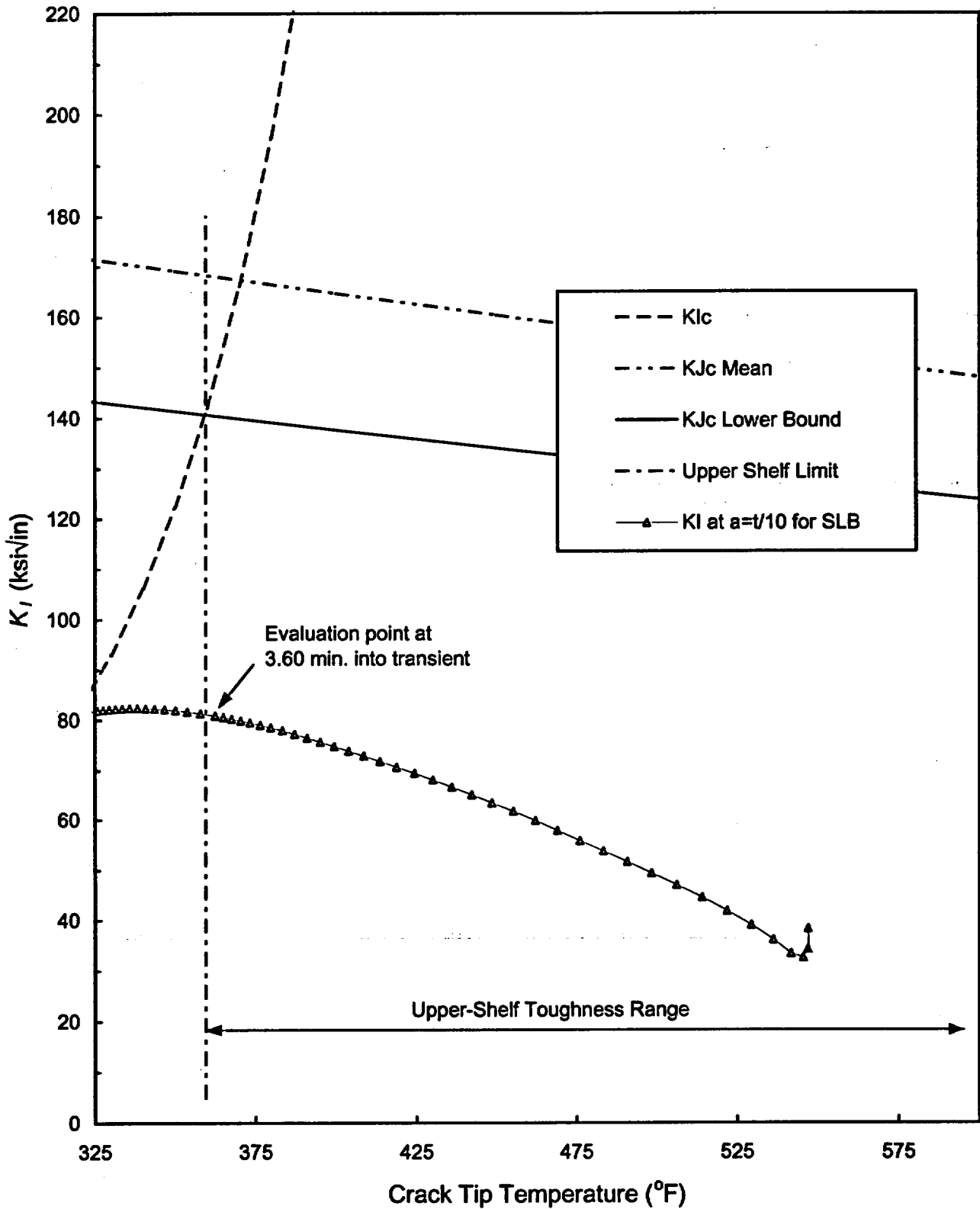
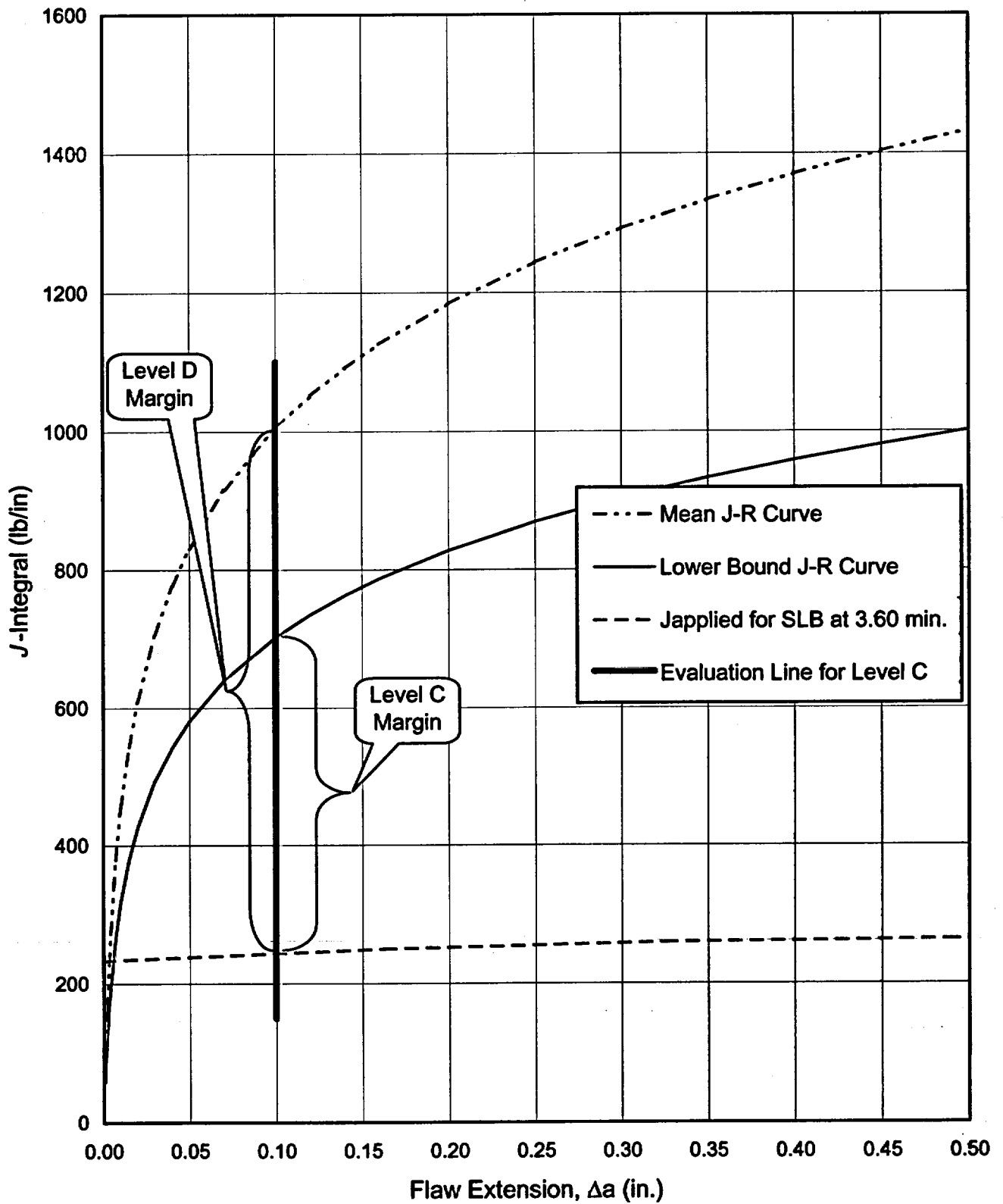




Figure 7-2 J-Integral vs. Flaw Extension for Levels C & D Service Loadings



## 8. Summary of Results

A low upper-shelf fracture mechanics analysis has been performed to evaluate the SA-847 circumferential reactor vessel weld at R. E. Ginna for projected low upper-shelf energy levels at 54 EFPY, considering Levels A, B, C, and D Service Loadings of the ASME Code.

Evidence that the ASME Code, Section XI, Appendix K [1] acceptance criteria have been satisfied for Levels A and B Service Loadings is provided by the following:

- (1) Figure 6-1 shows that with a factors of safety of 1.15 on pressure and 1.0 on thermal loading, the applied  $J$ -integral ( $J_1$ ) is less than the  $J$ -integral of the material at a ductile flaw extension of 0.10 in. ( $J_{0.1}$ ). The ratio  $J_{0.1}/J_1 = 5.79$  which is significantly greater than the required value of 1.0.
- (2) Figure 6-1 shows that with a factors of safety of 1.25 on pressure and 1.0 on thermal loading, flaw extensions are ductile and stable since the slope of the applied  $J$ -integral curve is less than the slope of the lower bound  $J$ - $R$  curve at the point where the two curves intersect.

Evidence that the ASME Code, Section XI, Appendix K [1] acceptance criteria have been satisfied for Levels C and D Service Loadings is provided by the following:

- (1) Figure 7-2 shows that with a factor of safety of 1.0 on loading, the applied  $J$ -integral ( $J_1$ ) is less than the  $J$ -integral of the material at a ductile flaw extension of 0.10 in. ( $J_{0.1}$ ). From Tables 7-4 and 7-5, the ratio  $J_{0.1}/J_1 = 703/243 = 2.89$ , which is much greater than the required value of 1.0.
- (2) Figure 7-2 shows that with a factor of safety of 1.0 on loading, flaw extensions are ductile and stable since the slope of the applied  $J$ -integral curve is less than the slopes of both the lower bound and mean  $J$ - $R$  curves at the points of intersection.
- (3) Figure 7-2 shows that flaw growth is stable at much less than 75% of the vessel wall thickness. It has also been shown that the remaining ligament is sufficient to preclude tensile instability by a large margin.

## 9. Conclusion

The limiting R. E. Ginna reactor vessel beltline weld satisfies the acceptance criteria of Appendix K to Section XI of the ASME Code [1] for projected low upper-shelf Charpy impact energy levels at 54 effective full power years of plant operation.

## 10. References

1. ASME Boiler and Pressure Vessel Code, Section XI, 1995 Edition with Addenda through 1996.
2. BAW-2192PA, Low Upper-Shelf Toughness Fracture Mechanics Analysis of Reactor Vessels of B&W Owners Reactor Vessel Working Group For Level A & B Service Loads, April 1994.
3. BAW-2275, Low Upper-Shelf Toughness Fracture Mechanics Analysis of B&W Designed Reactor Vessels for 48 EFPY, August 1996.
4. BAW-2178PA, Low Upper-Shelf Toughness Fracture Mechanics Analysis of Reactor Vessels of B&W Owners Reactor Vessel Working Group For Level C & D Service Loads, April 1994.
5. R. E. Ginna Nuclear Power Plant, Updated Final Safety Analysis Report, Revision 16, Volume 8, April 2001
6. WCAP-7254, Rochester Gas and Electric Robert E. Ginna Unit No. 1 Reactor Vessel Radiation Surveillance Program, May 1969.
7. ASME Boiler and Pressure Vessel Code, Section II, Part D, 1995 Edition with Addenda through 1996.
8. WCAP-13902, Analysis of Capsule S from the Rochester Gas and Electric Corporation R. E. Ginna Reactor Vessel Radiation Surveillance Program, December 1993.
9. G. Wrobel (RG&E) letter to J. R. Paljug (FRA-ANP), "RV Parameters," dated May 24, 2002 (attached as Appendix A).
10. USNRC Reactor Vessel Integrity Database (RVID) Version 2.0.1, U. S. Nuclear Regulatory Commission, July 2000.
11. Regulatory Guide 1.99, Revision 2, U.S. Nuclear Regulatory Commission, May 1988.
12. ASME Boiler and Pressure Vessel Code, Appendix K, Section XI, 2001 Edition.
13. EPRI NP-719-SR, T.U. Marston, Flaw Evaluation Procedures: ASME Section XI, Electric Power Research Institute, Palo Alto, California, August 1978.

11. Appendix A – G. Wrobel (RG&E) letter to J. R. Paljug (FRA-ANP), "RV Parameters,"

MAY-24-2002 10:18

RG&E GINNA ENGINEERING

716 771 3904 P.02



A Subsidiary of RGS Energy Group Inc.

ROCHESTER GAS AND ELECTRIC CORPORATION 89 EAST AVENUE, ROCHESTER, N.Y. 14649-0001 585-546-2700

[www.rge.com](http://www.rge.com)

GEORGE WROBEL  
Manager  
License Renewal

May 24, 2002

To: Joe Paljug  
From: George Wrobel  
Subject: RV Parameters

The reference for peak EOL neutron fluence at the reactor vessel beltline weld is WCAP-15885, Rev. 0, "R.E. Ginna Heatup and Cooldown Limit Curves for Normal Operation", May 2002.

In Table 6 of that WCAP, neutron fluence ( $E > 1.0$  MeV) is  $4.85 \text{ E} + 19$  at 52 EFPY, and  $5.01 \text{ E} + 19$  at 54 EFPY (attachment 1). The value of  $5.5 \text{ E} + 19$  used in the RV EMA is conservative with respect to these values.

The reference for initial  $RT_{\text{NDT}}$  of  $-4.8^\circ\text{F}$  is the RG&E "RCS Pressure and Temperature Limits Report PTLR", Rev. 3, 2/15/2001, Table PTLR-6 (attachment 2).

Table 6  
Summary of Calculated Maximum Pressure Vessel Exposure  
Clad/Basic Metal Interface

Neutron Fluence [E > 1.0 MeV]

Cumulative Operating Time [EFPY]	Neutron Fluence [n/cm <sup>2</sup> ]			
	0.0 Degrees	15.0 Degrees	30.0 Degrees	45.0 Degrees
24.8 (EOC 29)	2.68e+19	1.69e+19	1.22e+19	1.09e+19
28	2.94e+19	1.85e+19	1.34e+19	1.20e+19
32	3.26e+19	2.05e+19	1.48e+19	1.33e+19
36	3.57e+19	2.25e+19	1.63e+19	1.46e+19
40	3.89e+19	2.45e+19	1.77e+19	1.60e+19
44	4.21e+19	2.65e+19	1.92e+19	1.73e+19
48	4.53e+19	2.85e+19	2.07e+19	1.86e+19
52	4.85e+19	3.05e+19	2.21e+19	2.00e+19
54	5.01e+19	3.15e+19	2.28e+19	2.06e+19

Iron Atom Displacements

Cumulative Operating Time [EFPY]	Iron Atom Displacements [dpa]			
	0.0 Degrees	15.0 Degrees	30.0 Degrees	45.0 Degrees
24.8 (EOC 29)	4.37e-02	2.85e-02	2.01e-02	1.77e-02
28	4.79e-02	3.12e-02	2.20e-02	1.94e-02
32	5.31e-02	3.46e-02	2.44e-02	2.16e-02
36	5.82e-02	3.79e-02	2.68e-02	2.37e-02
40	6.34e-02	4.12e-02	2.91e-02	2.59e-02
44	6.86e-02	4.46e-02	3.15e-02	2.80e-02
48	7.38e-02	4.79e-02	3.39e-02	3.02e-02
52	7.89e-02	5.12e-02	3.63e-02	3.23e-02
54	8.15e-02	5.29e-02	3.75e-02	3.34e-02

**Table PTLR - 6**  
**Calculation of Adjusted Reference Temperatures at 28 EFY for the Limiting Reactor Vessel Material**

Parameter	Values	
	28 EFY	
Operating Time	Circ. Weld	Circ. Weld
Material	1/4-T	3/4-T
Location	1/4-T	3/4-T
Chemistry Factor (CF), °F <sup>(a)</sup>	160.7	160.7
Fluence (f), 10 <sup>19</sup> n/cm <sup>2</sup> (E > 1.0 MeV) <sup>(b)</sup>	2.11	.965
Fluence Factor (FF)	1.20	1.00
$\Delta RT_{NDT} = CF \times FF$ , °F	192.8	160.7
Initial $RT_{NDT}$ (I), °F	-4.8	-4.8
Margin (M), °F <sup>(b)</sup>	48.3	48.3
$ART = I + (CF \times FF) + M$ , °F <sup>(c)</sup>	236.3	204.2

(a) Values from Table PTLR - 3.

(b) Value calculated using Table PTLR - 5 values.

(c) Reference 1.

**ENCLOSURE 2**

**Westinghouse Non-Proprietary Class 3**

**WCAP-15885  
Revision 0**

**July 2002**

# **R. E. Ginna Heatup and Cooldown Limit Curves for Normal Operation**





---

## 3 RADIATION ANALYSIS AND NEUTRON DOSIMETRY

### 3.1 INTRODUCTION

This section describes a discrete ordinates  $S_n$  transport analysis performed for the R. E. Ginna reactor to determine the neutron radiation environment within the reactor pressure vessel and surveillance capsules. In this evaluation, fast neutron exposure parameters in terms of fast neutron fluence ( $E > 1.0$  MeV) and iron atom displacements (dpa) were established on a plant and fuel cycle specific basis for the first twenty nine reactor operating cycles. In addition, neutron dosimetry sensor sets from the first four surveillance capsules withdrawn from the R. E. Ginna reactor were re-analyzed using current dosimetry evaluation methodology. The results of these dosimetry re-evaluations provided a validation of the plant specific neutron transport calculations. The validated calculations were then used to project future fluence accumulation through operating periods extending to 54 effective full power years (efpy).

The use of fast neutron fluence ( $E > 1.0$  MeV) to correlate measured material property changes to the neutron exposure of the material has traditionally been accepted for development of damage trend curves as well as for the implementation of trend curve data to assess vessel condition. In recent years, however, it has been suggested that an exposure model that accounts for differences in neutron energy spectra between surveillance capsule locations and positions within the vessel wall could lead to an improvement in the uncertainties associated with damage trend curves as well as to a more accurate evaluation of damage gradients through the reactor vessel wall.

Because of this potential shift away from a threshold fluence toward an energy dependent damage function for data correlation, ASTM Standard Practice E853, "Analysis and Interpretation of Light-Water Reactor Surveillance Results," recommends reporting displacements per iron atom (dpa) along with fluence ( $E > 1.0$  MeV) to provide a data base for future reference. The energy dependent dpa function to be used for this evaluation is specified in ASTM Standard Practice E693, "Characterizing Neutron Exposures in Iron and Low Alloy Steels in Terms of Displacements per Atom." The application of the dpa parameter to the assessment of embrittlement gradients through the thickness of the reactor vessel wall has already been promulgated in Revision 2 to Regulatory Guide 1.99, "Radiation Embrittlement of Reactor Vessel Materials." Therefore, in keeping with the philosophy espoused in the current standards governing pressure vessel exposure evaluations, dpa data is also included in this section.

All of the calculations and dosimetry evaluations described in this report were based on the latest available nuclear cross-section data derived from ENDF/B-VI and made use of the latest available calculational tools. Furthermore, the neutron transport and dosimetry evaluation methodologies follow the guidance and meet the requirements of Regulatory Guide 1.190, "Calculational and Dosimetry Methods for Determining Pressure Vessel Neutron Fluence."<sup>(1)</sup> Additionally, the methods used to determine the pressure vessel neutron exposure are consistent with the NRC approved methodology described in WCAP-14040-NP-A, "Methodology Used to Develop Cold Overpressure Mitigating System Setpoints and RCS Heatup and Cooldown Limit Curves," January 1996.<sup>(2)</sup>

---

## 3.2 NEUTRON TRANSPORT CALCULATIONS

In performing the fast neutron exposure evaluations for the R. E. Ginna surveillance capsules and reactor vessel, plant specific forward transport calculations were carried out using the following three-dimensional flux synthesis technique:

$$\phi(r, \theta, z) = \phi(r, \theta) * \frac{\phi(r, z)}{\phi(r)}$$

where  $\phi(r, \theta, z)$  is the synthesized three-dimensional neutron flux distribution,  $\phi(r, \theta)$  is the transport solution in  $r, \theta$  geometry,  $\phi(r, z)$  is the two-dimensional solution for a cylindrical reactor model using the actual axial core power distribution, and  $\phi(r)$  is the one-dimensional solution for a cylindrical reactor model using the same source per unit height as that used in the  $r, \theta$  two-dimensional calculation.

For the R. E. Ginna analysis, all of the transport calculations were carried out using the DORT two-dimensional discrete ordinates code Version 3.1<sup>[13]</sup> and the BUGLE-96 cross-section library<sup>[14]</sup>. The BUGLE-96 library provides a 67 group coupled neutron-gamma ray cross-section data set produced specifically for light water reactor application. In these analyses, anisotropic scattering was treated with a  $P_3$  legendre expansion and the angular discretization was modeled with an  $S_{16}$  order of angular quadrature.

A plan view of the  $r, \theta$  model of the R. E. Ginna reactor geometry at the core midplane is shown in Figure 1. Since the reactor exhibits octant symmetry only a  $0^\circ$  to  $45^\circ$  sector is depicted. In addition to the core, reactor internals, pressure vessel and primary biological shield, the model also included explicit representations of the surveillance capsules, the pressure vessel cladding, and the insulation located external to the pressure vessel.

From a neutronic standpoint the inclusion of the surveillance capsules and associated support structure in the analytical model is significant. Since the presence of the capsules and structure has a marked impact on the magnitude of the neutron flux as well as on the relative neutron and gamma ray spectra at dosimetry locations within the capsules, a meaningful evaluation of the radiation environment internal to the capsules can be made only when these perturbation effects are properly accounted for in the analysis.

In developing the  $r, \theta$  analytical model of the reactor geometry shown in Figure 1, nominal design dimensions were employed for the various structural components. Likewise, water temperatures and, hence, coolant density in the reactor core and downcomer regions of the reactor were taken to be representative of full power operating conditions. The reactor core itself was treated as a homogeneous mixture of fuel, cladding, water, and miscellaneous core structures such as fuel assembly grids, guide tubes, etc. The  $r, \theta$  geometric mesh description of the reactor model shown in Figure 3.2-1 consisted of 170 radial by 67 azimuthal intervals. Mesh sizes were chosen to assure that proper convergence of the inner iterations was achieved on a pointwise basis. The pointwise inner iteration flux convergence criterion utilized in the  $r, \theta$  calculations was set at a value of 0.001.

A section view of the  $r, z$  model of the R. E. Ginna reactor is shown in Figure 2. The model extended radially from the centerline of the reactor core out to a location interior to the primary biological shield and over an axial span from an elevation 1 foot below the active fuel to approximately 1 foot above the active fuel. As in the case of the  $r, \theta$  model, nominal design dimensions and full power coolant densities were

employed in the calculations. In this case, the homogenous core region was treated as an equivalent cylinder with a volume equal to that of the active core zone. The stainless steel former plates located between the core baffle and core barrel regions were also explicitly included in the model. The  $r,z$  geometric mesh description of the reactor model shown in Figure 2 consisted of 153 radial by 90 axial intervals. Mesh sizes were chosen to assure that proper convergence of the inner iterations was achieved on a pointwise basis. The pointwise inner iteration flux convergence criterion utilized in the  $r,z$  calculations was also set at a value of 0.001.

The one-dimensional radial model used in the synthesis procedure consisted of the same 153 radial mesh intervals included in the  $r,z$  model. Thus, radial synthesis factors could easily be determined on a meshwise basis throughout the entire geometry.

The core power distributions used in the plant specific transport analysis for the R. E. Ginna reactor were taken from the appropriate fuel cycle design reports for Cycles 1 through 29. The data extracted from the design reports represented cycle average relative assembly powers, burnups, and axial distributions. Therefore, the calculated results provided data in terms of fuel cycle averaged neutron flux which, when multiplied by the appropriate fuel cycle length, in turn, yielded the incremental fast neutron exposure for each fuel cycle. In constructing the core source distributions, the energy distribution of the source was based on an appropriate fission split for uranium and plutonium isotopes; and from that fission split, composite values of energy release per fission, neutron yield per fission, and fission spectrum were determined. Fluence projections beyond the end of Cycle 29 were based on the assumption that the core power distribution averaged over Cycles 26 through 29 would be representative of future plant operation. Cycles 26 through 29 were designed as 18 month fuel cycles using the low leakage fuel management concept.

The maximum calculated fast neutron fluence ( $E > 1.0$  MeV) and dpa exposure values for the R. E. Ginna pressure vessel are provided in Table 6. As presented, these data represent the maximum exposure of the pressure vessel clad/base metal interface at azimuthal angles of 0, 15, 30, and 45 degrees relative to the core cardinal axes. The data tabulation includes the plant specific calculated fluence at the end of cycle twenty nine (the last cycle completed at the R. E. Ginna plant) and projections for future operation to 28, 32, 36, 40, 44, 48, 52, and 54 EFPY. Similar data applicable to the intermediate shell to nozzle shell circumferential weld as well as to the nozzle shell course located above the top of the active fuel stack are given in Table 7.

The results of the updated fluence calculations for the four surveillance capsules withdrawn to date from the R. E. Ginna reactor are provided in Table 8. These calculated values of neutron fluence should be used to specify the neutron exposure of the irradiated test specimens for use in materials damage correlations.

Updated lead factors for the R. E. Ginna surveillance capsules are provided in Table 9. The capsule lead factor is defined as the ratio of the calculated fluence at the geometric center of the surveillance capsule to the corresponding maximum calculated fluence at the pressure vessel clad/base metal interface.

In Table 9, the lead factors for capsules that have been withdrawn from the reactor (V, R, T, and S) were based on the calculated fluence values for the irradiation period corresponding to the time of withdrawal for the individual capsules. For the capsules remaining in the reactor (P and N), the lead factors correspond to the calculated fluence values at the projected end of cycle twenty nine, the last fuel cycle completed at the time of analysis. The lead factors provided in Table 9 should be used as the basis for the development of future capsule withdrawal schedules for the R. E. Ginna reactor.

Figure 1  
R. E. Ginna  $r,\theta$  Reactor Geometry at the Core Midplane

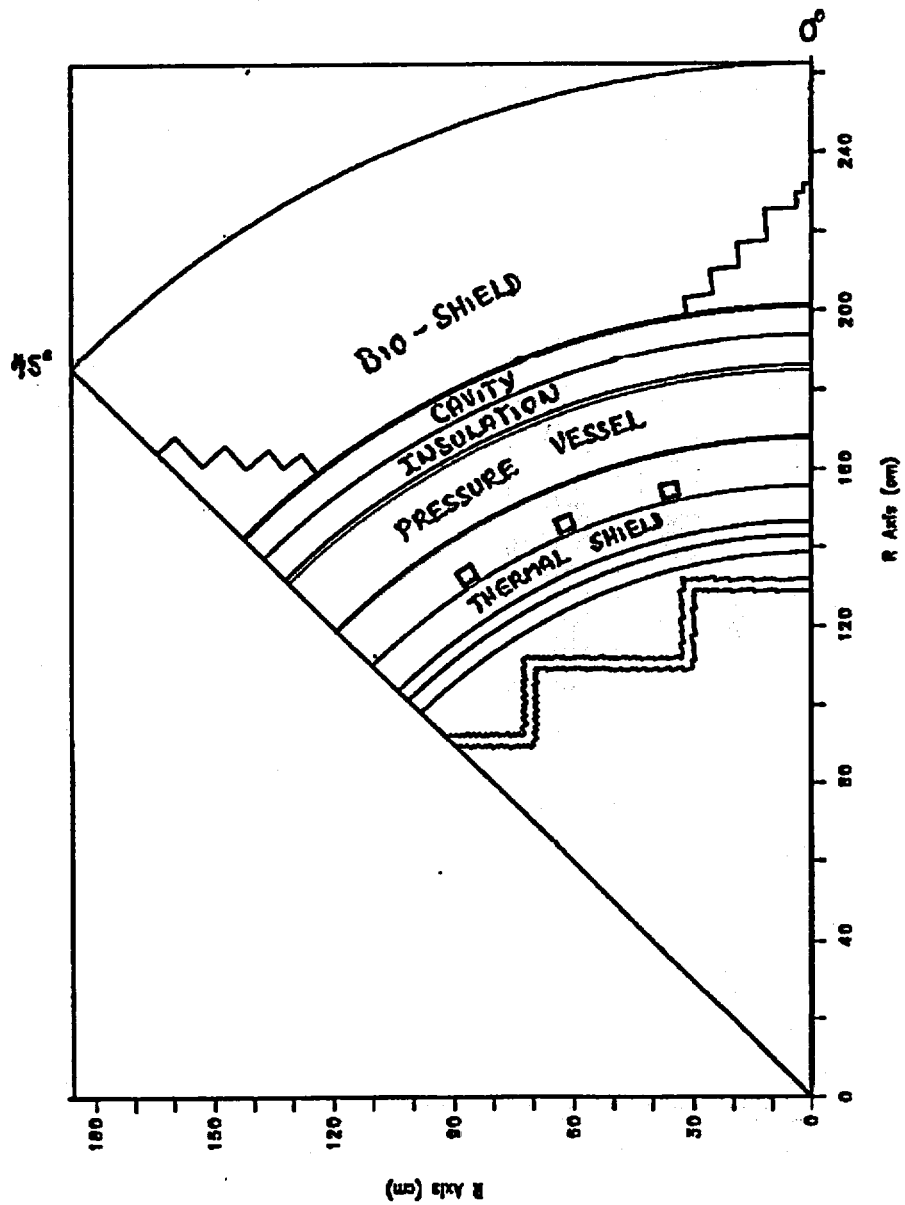
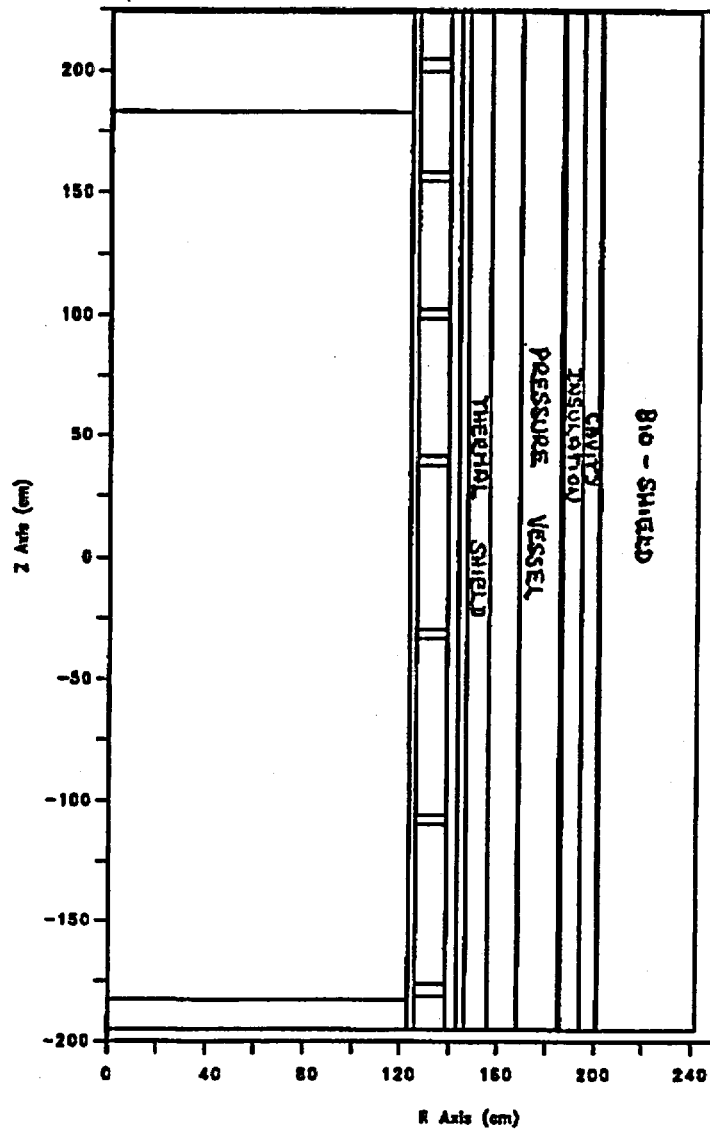


Figure 2  
R. E. Ginna r,z Geometry



**Table 6**  
**Summary of Calculated Maximum Pressure Vessel Exposure**  
**Clad/Base Metal Interface**

Neutron Fluence [E > 1.0 MeV]

Cumulative Operating Time [EFPY]	Neutron Fluence [n/cm <sup>2</sup> ]			
	0.0 Degrees	15.0 Degrees	30.0 Degrees	45.0 Degrees
24.8 (EOC 29)	2.68e+19	1.69e+19	1.22e+19	1.09e+19
28	2.94e+19	1.85e+19	1.34e+19	1.20e+19
32	3.26e+19	2.05e+19	1.48e+19	1.33e+19
36	3.57e+19	2.25e+19	1.63e+19	1.46e+19
40	3.89e+19	2.45e+19	1.77e+19	1.60e+19
44	4.21e+19	2.65e+19	1.92e+19	1.73e+19
48	4.53e+19	2.85e+19	2.07e+19	1.86e+19
52	4.85e+19	3.05e+19	2.21e+19	2.00e+19
54	5.01e+19	3.15e+19	2.28e+19	2.06e+19

Iron Atom Displacements

Cumulative Operating Time [EFPY]	Iron Atom Displacements [dpa]			
	0.0 Degrees	15.0 Degrees	30.0 Degrees	45.0 Degrees
24.8 (EOC 29)	4.37e-02	2.85e-02	2.01e-02	1.77e-02
28	4.79e-02	3.12e-02	2.20e-02	1.94e-02
32	5.31e-02	3.46e-02	2.44e-02	2.16e-02
36	5.82e-02	3.79e-02	2.68e-02	2.37e-02
40	6.34e-02	4.12e-02	2.91e-02	2.59e-02
44	6.86e-02	4.46e-02	3.15e-02	2.80e-02
48	7.38e-02	4.79e-02	3.39e-02	3.02e-02
52	7.89e-02	5.12e-02	3.63e-02	3.23e-02
54	8.15e-02	5.29e-02	3.75e-02	3.34e-02

Table 7

**Summary of Calculated Maximum Exposure of the Intermediate to Nozzle Shell  
Circumferential Weld and the Nozzle Shell Course  
Clad/Base Metal Interface**

**Neutron Fluence [E > 1.0 MeV]**

Cumulative Operating Time [EFPY]	Neutron Fluence [n/cm <sup>2</sup> ]			
	0.0 Degrees	15.0 Degrees	30.0 Degrees	45.0 Degrees
24.8 (EOC 29)	1.05e+18	6.64e+17	4.78e+17	4.26e+17
28	1.16e+18	7.28e+17	5.25e+17	4.68e+17
32	1.28e+18	8.07e+17	5.83e+17	5.21e+17
36	1.41e+18	8.86e+17	6.41e+17	5.74e+17
40	1.54e+18	9.65e+17	6.98e+17	6.27e+17
44	1.66e+18	1.04e+18	7.56e+17	6.80e+17
48	1.79e+18	1.12e+18	8.14e+17	7.32e+17
52	1.92e+18	1.20e+18	8.72e+17	7.85e+17
54	1.98e+18	1.24e+18	9.00e+17	8.12e+17

**Iron Atom Displacements**

Cumulative Operating Time [EFPY]	Iron Atom Displacements [dpa]			
	0.0 Degrees	15.0 Degrees	30.0 Degrees	45.0 Degrees
24.8 (EOC 29)	1.83e-03	1.19e-03	8.38e-04	7.35e-04
28	2.01e-03	1.31e-03	9.20e-04	8.09e-04
32	2.23e-03	1.45e-03	1.02e-03	9.01e-04
36	2.45e-03	1.59e-03	1.12e-03	9.92e-04
40	2.67e-03	1.73e-03	1.22e-03	1.08e-03
44	2.89e-03	1.87e-03	1.33e-03	1.17e-03
48	3.11e-03	2.02e-03	1.43e-03	1.27e-03
52	3.33e-03	2.16e-03	1.53e-03	1.36e-03
54	3.44e-03	2.23e-03	1.58e-03	1.40e-03

**Table 8**  
**Calculated Surveillance Capsule Exposure**

<b>Capsule</b>	<b>Irradiation Time [EFPY]</b>	<b>Fluence (E &gt; 1.0 MeV) [n/cm<sup>2</sup>]</b>	<b>Iron Displacements [dpa]</b>
V	1.4	5.87e+18	1.07e-02
R	2.6	1.02e+19	1.85e-02
T	6.9	1.69e+19	2.94e-02
S	17.0	3.64e+19	6.38e-02

**Table 9**  
**Calculated Surveillance Capsule Lead Factors**

<b>Capsule ID And Location</b>	<b>Status</b>	<b>Lead Factor</b>
V (13°)	Withdrawn EOC 1	2.96
R (13°)	Withdrawn EOC 3	2.97
T (23°)	Withdrawn EOC 9	1.82
S (33°)	Withdrawn EOC 22	1.79
P (23°)	In Reactor	1.91
N (33°)	In Reactor	1.81

Note: Lead factors for capsules remaining in the reactor are based on cycle specific exposure calculations through fuel cycle twenty nine.



### 3.3 NEUTRON DOSIMETRY EVALUATIONS

#### 3.3.1 Sensor Reaction Rate Determinations

In this section, the results of the evaluations of the four neutron sensor sets withdrawn as a part of the R. E. Ginna Reactor Vessel Materials Surveillance Program are presented. The capsule designation, location within the reactor, and time of withdrawal of each of these dosimetry sets were as follows:

Capsule ID	Azimuthal Location	Withdrawal Time	Irradiation Time [efps]
V	13°	End of Cycle 1	4.46e+07
R	13°	End of Cycle 3	8.05e+07
T	23°	End of Cycle 9	2.17e+08
S	33°	End of Cycle 22	5.36e+08

The type and radial locations of the neutron sensors within the capsules are summarized as follows:

Sensor Type	Radius [cm]
Copper	158.11
Iron - Core Side Charpy	158.11
Iron - Vessel Side Charpy	159.11
Nickel	158.91
Uranium 238	158.35
Neptunium 237	158.35
Bare Cobalt-Aluminum	159.11
Cd Cov. Cobalt-Aluminum	159.11

The copper, nickel, and cobalt-aluminum monitors, in wire form, were placed in holes drilled in spacers at several axial levels within the capsules. The cadmium shielded uranium and neptunium fission monitors were accommodated within the dosimeter block located near the center of the capsule. The iron sensors were obtained by cutting small samples from individual charpy specimens taken from several locations within the surveillance capsules.

The use of passive monitors such as those listed above does not yield a direct measure of the energy dependent neutron flux at the point of interest. Rather, the activation or fission process is a measure of the integrated effect that the time and energy dependent neutron flux has on the target material over the course of the irradiation period. An accurate assessment of the average neutron flux level incident on the various monitors may be derived from the activation measurements only if the irradiation parameters are well known. In particular, the following variables are of interest:

- The measured specific activity of each monitor,
- The physical characteristics of each monitor,
- The operating history of the reactor,
- The energy response of each monitor, and
- The neutron energy spectrum at the monitor location.

The radiometric counting of each of the R. E. Ginna dosimetry data sets was accomplished by Westinghouse using established ASTM procedures. Following sample preparation and weighing, the activity of each monitor was determined by means of a high resolution gamma spectrometer. For the copper, iron, nickel, and cobalt-aluminum sensors, these analyses were performed by direct counting of each of the individual samples. In the case of the uranium and neptunium fission sensors, the analyses were carried out by direct counting preceded by dissolution and chemical separation of cesium from the sensor material.

The irradiation history of the reactor over the irradiation period experienced by Capsules V, R, T, and S was obtained on a monthly basis from reactor startup to the end of the dosimetry evaluation period. For the sensor sets utilized in the surveillance capsules, the half-lives of the product isotopes are long enough that a monthly histogram describing reactor operation has proven to be an adequate representation for use in radioactive decay corrections for the reactions of interest in the exposure evaluations.

Having the measured specific activities, the operating history of the reactor, and the physical characteristics of the sensors, reaction rates referenced to full power operation were determined from the following equation:

$$R = \frac{A}{N_0 F Y \sum_{j=1}^n \frac{P_j}{P_{ref}} C_j (1 - e^{-\lambda_j}) e^{-\lambda_j t}}$$

where:

- A = measured specific activity (dps/g)  
 R = reaction rate averaged over the irradiation period and referenced to operation at a core power level of  $P_{ref}$  (rps/nucleus).  
 $N_0$  = number of target element atoms per gram of sensor.

$F$	=	weight fraction of the target isotope in the sensor material.
$Y$	=	number of product atoms produced per reaction.
$P_j$	=	average core power level during irradiation period $j$ (MW).
$P_{ref}$	=	maximum or reference core power level of the reactor (MW).
$C_j$	=	calculated ratio of $\phi(E \geq 1.0 \text{ MeV})$ during irradiation period $j$ to the time weighted average $\phi(E \geq 1.0 \text{ MeV})$ over the entire irradiation period.
$\lambda$	=	decay constant of the product isotope ( $s^{-1}$ ).
$t_j$	=	length of irradiation period $j$ (s).
$t_d$	=	decay time following irradiation period $j$ (s).

and the summation is carried out over the total number of monthly intervals comprising the irradiation period.

In the above equation, the ratio  $P_j/P_{ref}$  accounts for month by month variation of power level within a given fuel cycle. The ratio  $C_j$  is calculated for each fuel cycle using the methodology described in Section 3.2 of this report and accounts for the change in sensor reaction rates caused by variations in flux level due to changes in core power spatial distributions from fuel cycle to fuel cycle. For a single cycle irradiation  $C_j = 1.0$ . However, for multiple cycle irradiations, particularly those employing low leakage fuel management, the additional  $C_j$  correction must be utilized. This additional correction can be quite significant for sensor sets that have been irradiated for many fuel cycles in a reactor that has transitioned from non-low leakage to low leakage fuel management.

Prior to using the measured reaction rates in the least squares adjustment procedure discussed later in this section, additional corrections were made to  $U^{238}$  measurements to account for the presence of  $U^{235}$  impurities in the sensors as well as to adjust for the build-in of plutonium isotopes over the course of the irradiation. These corrections were location and fluence dependent and were derived from the plant specific discrete ordinates analysis described in Section 3.2. Corrections were also made to the  $U^{238}$  and  $Np^{237}$  sensor reaction rates to account for gamma ray induced fission reactions that occurred over the course of the irradiation. These photo-fission corrections were, likewise, location dependent and were based on the transport calculations described in Section 3.2.

Results of the sensor reaction rate determinations for Capsules V, R, T, and S are given in Tables 10 through 14. In Tables 10 through 13, the measured specific activities, gradient corrected specific activities, and decay corrected reaction rates are listed for Capsules V, R, T, and S, respectively. A summary of the reaction rates for each capsule is provided in Table 14. The data listed in Table 14 are indexed to the geometric center of the respective capsules and included all corrections for  $U^{235}$  impurities, Pu build-in, and photo-fission effects.

**Table 10**  
**Measured Sensor Specific Activities and Reaction Rates**  
**Capsule V**

Sample ID	Foil ID	Radius [cm.]	Measured Activity [dps/g]	Saturated Activity [dps/g]	Radially Adjusted Saturated Activity [dps/g]	Radially Adjusted Reaction Rate [rps/atom]	Average Reaction Rate [rps/atom]
CU	Top	158.11	7.38E+04	4.63E+05	4.43E+05	6.77E-17	
CU	Top-Mid	158.11	6.77E+04	4.25E+05	4.07E+05	6.21E-17	
CU	Bot-Mid	158.11	7.48E+04	4.70E+05	4.49E+05	6.86E-17	
CU	Bottom	158.11	8.13E+04	5.10E+05	4.89E+05	7.45E-17	6.82E-17
FE	W-1	158.11	2.47E+06	5.00E+06	4.82E+06	7.64E-15	
FE	R-1	158.11	2.57E+06	5.20E+06	5.02E+06	7.95E-15	
FE	S-6	158.11	2.18E+06	4.41E+06	4.25E+06	6.74E-15	
FE	P-7	158.11	2.57E+06	5.20E+06	5.02E+06	7.95E-15	
FE	W-2	159.11	2.04E+06	4.13E+06	4.78E+06	7.58E-15	
FE	R-3	159.11	1.95E+06	3.95E+06	4.57E+06	7.25E-15	
FE	S-8	159.11	2.02E+06	4.09E+06	4.74E+06	7.51E-15	
FE	P-9	159.11	2.10E+06	4.25E+06	4.92E+06	7.80E-15	7.55E-15
NI	Middle	158.11	2.38E+07	6.51E+07	6.21E+07	8.90E-15	8.90E-15
U	Middle	158.35	2.30E+05	7.26E+06	7.26E+06	4.77E-14	3.91E-14
NP	Middle	158.35	1.23E+06	3.88E+07	3.88E+07	2.48E-13	2.44E-13

**Notes:**

- The average U-238(n,f) reaction rate of 2.91E-14 includes the correction of a factor of 0.861 to account for plutonium build-in and an additional factor of 0.950 to account for photo-fission effects in the sensor.
- The average Np-237(n,f) reaction rate of 2.44E-13 includes the correction of a factor of 0.983 to account for the photo-fission effects in the sensor.

**Table 11**  
**Measured Sensor Specific Activities and Reaction Rates**  
**Capsule R**

Sample ID	Foil ID	Radius [cm.]	Measured Activity [dps/g]	Saturated Activity [dps/g]	Radially Adjusted Saturated Activity [dps/g]	Radially Adjusted Reaction Rate [rps/atom]	Average Reaction Rate [rps/atom]
74-2204	Top	158.11	1.08E+05	4.42E+05	4.23E+05	6.45E-17	
74-2207	Top-Mid	158.11	9.68E+04	3.96E+05	3.79E+05	5.78E-17	
74-2213	Bot-Mid	158.11	1.15E+05	4.70E+05	4.50E+05	6.87E-17	
74-2216	Bottom	158.11	1.15E+05	4.70E+05	4.50E+05	6.87E-17	6.49E-17
74-2202	W-13	158.11	2.08E+06	5.19E+06	5.00E+06	7.93E-15	
74-2200	R-14	158.11	1.98E+06	4.94E+06	4.76E+06	7.55E-15	
74-2198	P-18	158.11	2.06E+06	5.14E+06	4.95E+06	7.85E-15	
74-2203	W-14	159.11	1.63E+06	4.07E+06	4.71E+06	7.46E-15	
74-2201	R-15	159.11	1.70E+06	4.24E+06	4.91E+06	7.78E-15	
74-2199	P-19	159.11	1.85E+06	4.61E+06	5.34E+06	8.47E-15	7.84E-15
74-2210	Middle	158.11	5.83E+06	7.36E+07	7.03E+07	1.01E-14	1.01E-14
74-2220	Middle	158.35	4.32E+05	7.79E+06	7.79E+06	5.12E-14	4.11E-14
74-2219	Middle	158.35	4.25E+06	7.66E+07	7.66E+07	4.89E-13	4.81E-13
74-2205	Top	159.11	3.09E+07	1.26E+08	1.22E+08	7.97E-12	
74-2208	Top-Mid	159.11	3.14E+07	1.28E+08	1.24E+08	8.10E-12	
74-2211	Middle	159.11	2.96E+07	1.21E+08	1.17E+08	7.64E-12	
74-2214	Bot-Mid	159.11	2.94E+07	1.20E+08	1.16E+08	7.59E-12	
74-2217	Bottom	159.11	2.94E+07	1.20E+08	1.16E+08	7.59E-12	7.78E-12
74-2206	Top	159.11	1.19E+07	4.87E+07	5.69E+07	3.71E-12	
74-2209	Top-Mid	159.11	1.18E+07	4.83E+07	5.64E+07	3.68E-12	
74-2212	Middle	159.11	1.07E+07	4.38E+07	5.11E+07	3.34E-12	
74-2215	Bot-Mid	159.11	1.24E+07	5.07E+07	5.92E+07	3.87E-12	
74-2218	Bottom	159.11	1.24E+07	5.07E+07	5.92E+07	3.87E-12	3.69E-12

**Notes:**

- The average U-238(n,f) reaction rate of 4.11E-14 includes the correction of a factor of 0.845 to account for plutonium build-in and an additional factor of 0.950 to account for photo-fission effects in the sensor.
- The average Np-237(n,f) reaction rate of 4.81E-13 includes the correction of a factor of 0.983 to account for the photo-fission effects in the sensor.

Table 12  
Measured Sensor Specific Activities and Reaction Rates  
Capsule T

Sample ID	Foil ID	Radius [cm.]	Measured Activity [dps/g]	Saturated Activity [dps/g]	Radially Adjusted Saturated Activity [dps/g]	Radially Adjusted Reaction Rate [rps/atom]	Average Reaction Rate [rps/atom]
81-1392	Top	158.11	1.60E+05	3.51E+05	3.35E+05	5.11E-17	
81-1395	Top-Mid	158.11	1.40E+05	3.07E+05	2.93E+05	4.47E-17	
81-1402	Bot-Mid	158.11	1.66E+05	3.64E+05	3.48E+05	5.30E-17	
81-1415	Bottom	158.11	1.74E+05	3.82E+05	3.64E+05	5.56E-17	5.11E-17
81-3390	S-22	158.11	1.14E+06	3.36E+06	3.19E+06	5.06E-15	
81-3392	P-28	158.11	1.27E+06	3.74E+06	3.56E+06	5.64E-15	
81-3394	W-21	158.11	1.30E+06	3.83E+06	3.64E+06	5.77E-15	
81-3391	S-23	159.11	1.01E+06	2.97E+06	3.43E+06	5.44E-15	
81-3393	P-29	159.11	1.03E+06	3.03E+06	3.50E+06	5.55E-15	
81-3395	W-22	159.11	1.10E+06	3.24E+06	3.74E+06	5.92E-15	5.56E-15
81-1399	Middle	158.11	8.62E+05	5.25E+07	5.01E+07	7.17E-15	7.17E-15
81-1388	Middle	158.35	7.41E+05	5.34E+06	5.34E+06	3.51E-14	2.74E-14
81-1389	Middle	158.35	6.09E+06	4.39E+07	4.39E+07	2.80E-13	2.75E-13
81-1390	Top	159.11	3.17E+07	6.96E+07	6.60E+07	4.31E-12	
81-1393	Top-Mid	159.11	3.06E+07	6.72E+07	6.37E+07	4.16E-12	
81-1396	Middle	159.11	3.03E+07	6.65E+07	6.31E+07	4.12E-12	
81-1400	Bot-Mid	159.11	3.27E+07	7.18E+07	6.81E+07	4.44E-12	
81-1403	Bottom	159.11	3.07E+07	6.74E+07	6.39E+07	4.17E-12	4.24E-12
81-1391	Top	159.11	1.21E+07	2.66E+07	3.06E+07	2.00E-12	
81-1394	Top-Mid	159.11	1.13E+07	2.48E+07	2.86E+07	1.87E-12	
81-1397	Middle	159.11	1.16E+07	2.55E+07	2.94E+07	1.92E-12	
81-1401	Bot-Mid	159.11	1.26E+07	2.77E+07	3.19E+07	2.08E-12	
81-1404	Bottom	159.11	1.20E+07	2.63E+07	3.04E+07	1.98E-12	1.97E-12

Notes:

- The average U-238(n,f) reaction rate of 2.74E-14 includes the correction of a factor of 0.820 to account for plutonium build-in and an additional factor of 0.955 to account for photo-fission effects in the sensor.
- The average Np-237(n,f) reaction rate of 2.75E-13 includes the correction of a factor of 0.984 to account for the photo-fission effects in the sensor.

Table 13  
Measured Sensor Specific Activities and Reaction Rates  
Capsule S

Sample ID	Foil ID	Radius [cm.]	Measured Activity [dps/g]	Saturated Activity [dps/g]	Radially Adjusted Saturated Activity [dps/g]	Radially Adjusted Reaction Rate [rps/atom]	Average Reaction Rate [rps/atom]
93-3163	Top	158.11	2.06E+05	3.06E+05	2.92E+05	4.45E-17	
93-3166	Top-Mid	158.11	1.82E+05	2.70E+05	2.58E+05	3.93E-17	
93-3172	Bot-Mid	158.11	1.98E+05	2.94E+05	2.81E+05	4.28E-17	
93-3175	Bottom	158.11	2.18E+05	3.24E+05	3.09E+05	4.71E-17	4.34E-17
93-4326	P-31	158.11	1.62E+06	2.93E+06	2.79E+06	4.42E-15	4.42E-15
93-3169	Middle	158.11	8.51E+06	4.27E+07	4.06E+07	5.81E-15	5.81E-15
93-3159	Middle	158.35	1.40E+06	4.63E+06	4.63E+06	3.04E-14	2.19E-14
93-3160	Middle	158.35	1.11E+07	3.67E+07	3.67E+07	2.34E-13	2.30E-13
93-3161	Top	159.11	3.55E+07	5.27E+07	5.05E+07	3.29E-12	
93-3164	Top-Mid	159.11	3.71E+07	5.51E+07	5.28E+07	3.44E-12	
93-3167	Middle	159.11	3.39E+07	5.03E+07	4.82E+07	3.15E-12	
93-3170	Bot-Mid	159.11	3.60E+07	5.35E+07	5.12E+07	3.34E-12	
93-3173	Bottom	159.11	3.45E+07	5.12E+07	4.91E+07	3.20E-12	3.29E-12
93-3162	Top	159.11	1.43E+07	2.12E+07	2.47E+07	1.61E-12	
93-3165	Top-Mid	159.11	1.37E+07	2.03E+07	2.37E+07	1.54E-12	
93-3168	Middle	159.11	1.31E+07	1.95E+07	2.26E+07	1.48E-12	
93-3171	Bot-Mid	159.11	1.45E+07	2.15E+07	2.50E+07	1.63E-12	
93-3174	Bottom	159.11	1.35E+07	2.00E+07	2.33E+07	1.52E-12	1.56E-12

**Notes:**

- The average U-238(n,f) reaction rate of 2.19E-14 includes the correction of a factor of 0.755 to account for plutonium build-in and an additional factor of 0.953 to account for photo-fission effects in the sensor.
- The average Np-237(n,f) reaction rate of 2.30E-13 includes the correction of a factor of 0.983 to account for the photo-fission effects in the sensor.

Table 14  
 Summary of Sensor Reaction Rates from Capsules V, R, T, and S

Sensor Reaction	Measured Reaction Rate [rps/nucleus]			
	Capsule V	Capsule R	Capsule T	Capsule S
Cu-63(n, $\alpha$ )Co-60	6.82e-17	6.49e-17	5.11e-17	4.34e-17
Fe-54(n,p)Mn-54	7.55e-15	7.84e-15	5.56e-15	4.42e-15
Ni-58(n,p)Co-58	8.90e-15	1.01e-14	7.17e-15	5.81e-15
U-238(n,f)Cs-137 Cd Covered	3.91e-14	4.11e-14	2.74e-14	2.19e-14
Np-237(n,f)Cs-137 Cd Covered	Rejected	4.81e-13	2.75e-13	2.30e-13
Co-59(n, $\gamma$ ) Co-60	None	7.78e-12	4.24e-12	3.29e-12
Co-59(n, $\gamma$ ) Co-60 Cd Covered	None	3.69e-12	1.97e-12	1.56e-12



### 3.4 LEAST SQUARES EVALUATION OF SENSOR SETS

Least squares adjustment methods provide the capability of combining the measurement data with the neutron transport calculation resulting in a Best Estimate neutron energy spectrum with associated uncertainties. Best Estimates for key exposure parameters such as  $\phi(E > 1.0 \text{ MeV})$  or dpa/s along with their uncertainties are then easily obtained from the adjusted spectrum. In general, the least squares methods, as applied to surveillance capsule dosimetry evaluations, act to reconcile the measured sensor reaction rate data, dosimetry reaction cross-sections, and the calculated neutron energy spectrum within their respective uncertainties. For example,

$$R_i \pm \delta_{R_i} = \sum_g (\sigma_{ig} \pm \delta_{\sigma_{ig}})(\phi_g \pm \delta_{\phi_g})$$

relates a set of measured reaction rates,  $R_i$ , to a single neutron spectrum,  $\phi_g$ , through the multigroup dosimeter reaction cross-section,  $\sigma_{ig}$ , each with an uncertainty  $\delta$ . The primary objective of the least squares evaluation is to produce unbiased estimates of the neutron exposure parameters at the location of the measurement.

For the least squares evaluation of the R. E. Ginna surveillance capsule dosimetry, The FERRET code<sup>[15]</sup> was employed to combine the results of the plant specific neutron transport calculations and sensor set reaction rate measurements to determine best estimate values of exposure parameters ( $\phi(E > 1.0 \text{ MeV})$  and dpa) along with associated uncertainties for the three in-vessel capsules withdrawn to date.

The application of the least squares methodology requires the following input:

- 1 - The calculated neutron energy spectrum and associated uncertainties at the measurement location.
- 2 - The measured reaction rates and associated uncertainty for each sensor contained in the multiple foil set.
- 3 - The energy dependent dosimetry reaction cross-sections and associated uncertainties for each sensor contained in the multiple foil sensor set.

For the R. E. Ginna application, the calculated neutron spectrum was obtained from the results of plant specific neutron transport calculations described in Section 3.2 of this report. The sensor reaction rates were derived from the measured specific activities using the procedures described in Section 3.3. The dosimetry reaction cross-sections and uncertainties were obtained from the SNLRML dosimetry cross-section library<sup>[16]</sup>. The SNLRML library is an evaluated dosimetry reaction cross-section compilation recommended for use in LWR evaluations by ASTM Standard E1018, "Application of ASTM Evaluated Cross-Section Data File, Matrix E 706 (IIB)".

The uncertainties associated with the measured reaction rates, dosimetry cross-sections, and calculated neutron spectrum were input to the least squares procedure in the form of variances and covariances. The assignment of the input uncertainties followed the guidance provided in ASTM Standard E 944, "Application of Neutron Spectrum Adjustment Methods in Reactor Surveillance."

The following provides a summary of the uncertainties associated with the least squares evaluation of the R. E. Ginna surveillance capsule sensor sets:

#### Reaction Rate Uncertainties

The overall uncertainty associated with the measured reaction rates includes components due to the basic measurement process, the irradiation history corrections, and the corrections for competing reactions. A high level of accuracy in the reaction rate determinations is assured by utilizing laboratory procedures that conform to the ASTM National Consensus Standards for reaction rate determinations for each sensor type.

After combining all of these uncertainty components, the sensor reaction rates derived from the counting and data evaluation procedures were assigned the following net uncertainties for input to the least squares evaluation:

Reaction	Uncertainty
$\text{Cu}^{63}(\text{n},\alpha)\text{Co}^{60}$	5%
$\text{Fe}^{54}(\text{n},\text{p})\text{Mn}^{54}$	5%
$\text{Ni}^{58}(\text{n},\text{p})\text{Co}^{58}$	5%
$\text{U}^{238}(\text{n},\text{f})\text{Cs}^{137}$	10%
$\text{Np}^{237}(\text{n},\text{f})\text{Cs}^{137}$	10%
$\text{Co}^{59}(\text{n},\gamma)\text{Co}^{60}$	5%

#### Dosimetry Cross-Section Uncertainties

The reaction rate cross-sections used in the least squares evaluations were taken from the SNLRML library. This data library provides reaction cross-sections and associated uncertainties, including covariances, for 66 dosimetry sensors in common use. Both cross-sections and uncertainties are provided in a fine multigroup structure for use in least squares adjustment applications. These cross-sections were compiled from the most recent cross-section evaluations and they have been tested with respect to their accuracy and consistency for least squares evaluations. Further, the library has been empirically tested for use in fission spectra determination as well as in the fluence and energy characterization of 14 MeV neutron sources. Detailed discussions of the contents of the SNLRML library along with the evaluation process for each of the sensors is provided in Reference 16.

For sensors included in the R. E. Ginna surveillance capsules, the following uncertainties in the fission spectrum averaged cross-sections are provided in the SNLRML documentation package.

Reaction	Uncertainty
$\text{Cu}^{63}(\text{n},\alpha)\text{Co}^{60}$	4.08-4.16%
$\text{Fe}^{54}(\text{n},\text{p})\text{Mn}^{54}$	3.05-3.11%
$\text{Ni}^{58}(\text{n},\text{p})\text{Co}^{58}$	4.49-4.56%
$\text{U}^{238}(\text{n},\text{f})\text{Cs}^{137}$	0.54-0.64%
$\text{Np}^{237}(\text{n},\text{f})\text{Cs}^{137}$	10.32-10.97%
$\text{Co}^{59}(\text{n},\gamma)\text{Co}^{60}$	0.79-3.59%

These tabulated ranges provide an indication of the dosimetry cross-section uncertainties associated with the sensor sets used in LWR irradiations.

### Calculated Neutron Spectrum

The neutron spectrum input to the least squares adjustment procedure was obtained directly from the results of plant specific transport calculations for each surveillance capsule location. The spectrum at each location was input in an absolute sense (rather than as simply a relative spectral shape). Therefore, within the constraints of the assigned uncertainties, the calculated data were treated equally with the measurements.

While the uncertainties associated with the reaction rates were obtained from the measurement procedures and counting benchmarks and the dosimetry cross-section uncertainties were supplied directly with the SNLRML library, the uncertainty matrix for the calculated spectrum was constructed from the following relationship:

$$M_{g'g} = R_n^2 + R_g * R_g * P_{g'g}$$

where  $R_n$  specifies an overall fractional normalization uncertainty and the fractional uncertainties  $R_g$  and  $R_g$  specify additional random groupwise uncertainties that are correlated with a correlation matrix given by:

$$P_{g'g} = [1 - \theta] * \delta_{g'g} + \theta * e^{-H}$$

where

$$H = \frac{(g - g')^2}{2\gamma^2}$$

The first term in the correlation matrix equation specifies purely random uncertainties, while the second term describes the short range correlations over a group range  $\gamma$  ( $\theta$  specifies the strength of the latter term). The value of  $\delta$  is 1.0 when  $g = g'$  and 0.0 otherwise.

The set of parameters defining the input covariance matrix for the R. E. Ginna calculated spectra was as follows:

Flux Normalization Uncertainty ( $R_n$ )	15%
Flux Group Uncertainties ( $R_g, R_g'$ )	
( $E > 0.0055$ MeV)	15%
( $0.68$ eV $< E < 0.0055$ MeV)	29%
( $E < 0.68$ eV)	52%
Short Range Correlation ( $\theta$ )	
( $E > 0.0055$ MeV)	0.9
( $0.68$ eV $< E < 0.0055$ MeV)	0.5
( $E < 0.68$ eV)	0.5
Flux Group Correlation Range ( $\gamma$ )	
( $E > 0.0055$ MeV)	6
( $0.68$ eV $< E < 0.0055$ MeV)	3
( $E < 0.68$ eV)	2

Results of the least squares evaluation of the four sensor sets withdrawn from the R. E. Ginna reactor are provided in Tables 15 and 16. In Table 15, measured, calculated, and best estimate sensor reaction rates are given for Capsules V, R, T, and S. The improvement in the fit of the adjusted spectra to the measurements is evident for all four capsule data sets. Prior to the application of the adjustment procedure M/C ratios for individual foil reactions ranged from 0.75 to 1.32, while after the adjustment M/BE ratios ranged from 0.91 to 1.12. Thus, demonstrating a significant improvement in the data fits.

In Table 16, the calculated and best estimate exposure rates and integrated exposures of Capsules V, R, T, and S are given. Data are provided in terms of both fluence ( $E > 1.0$  MeV) and iron atom displacements.

Table 15  
Comparison of Measured, Calculated, and Best Estimate  
Reaction Rates at the Surveillance Capsule Center

Surveillance Capsule V

Reaction	Reaction Rate [rps/atom]			M/C	M/BE
	Measured	Calculated	Best Estimate		
$\text{Cu}^{63}(\text{n},\alpha)\text{Co}^{60}$	6.82e-17	6.69e-17	6.54e-17	1.02	1.04
$\text{Fe}^{54}(\text{n},\text{p})\text{Mn}^{54}$	7.55e-15	8.14e-15	7.34e-15	0.93	1.03
$\text{Ni}^{58}(\text{n},\text{p})\text{Co}^{58}$	8.90e-15	1.14e-14	9.74e-15	0.78	0.91
$\text{U}^{238}(\text{n},\text{f})\text{Cs}^{137} \text{ Cd}$	3.91e-14	4.37e-14	3.77e-14	0.89	1.04
$\text{Np}^{237}(\text{n},\text{f})\text{Cs}^{137} \text{ Cd}$					
$\text{Co}^{59}(\text{n},\gamma)\text{Co}^{60}$					
$\text{Co}^{59}(\text{n},\gamma)\text{Co}^{60} \text{ Cd}$					

Surveillance Capsule R

Reaction	Reaction Rate [rps/atom]			M/C	M/BE
	Measured	Calculated	Best Estimate		
$\text{Cu}^{63}(\text{n},\alpha)\text{Co}^{60}$	6.49e-17	6.41e-17	6.39e-17	1.01	1.02
$\text{Fe}^{54}(\text{n},\text{p})\text{Mn}^{54}$	7.84e-15	7.79e-15	7.74e-15	1.01	1.01
$\text{Ni}^{58}(\text{n},\text{p})\text{Co}^{58}$	1.01e-14	1.09e-14	1.06e-14	0.93	0.95
$\text{U}^{238}(\text{n},\text{f})\text{Cs}^{137} \text{ Cd}$	4.11e-14	4.18e-14	4.22e-14	0.98	0.97
$\text{Np}^{237}(\text{n},\text{f})\text{Cs}^{137} \text{ Cd}$	4.81e-13	3.64e-13	4.28e-13	1.32	1.12
$\text{Co}^{59}(\text{n},\gamma)\text{Co}^{60}$	7.78e-12	9.22e-12	7.84e-12	0.84	0.99
$\text{Co}^{59}(\text{n},\gamma)\text{Co}^{60} \text{ Cd}$	3.69e-12	3.66e-12	3.68e-12	1.01	1.00

Surveillance Capsule T

Reaction	Reaction Rate [rps/atom]			M/C	M/BE
	Measured	Calculated	Best Estimate		
$\text{Cu}^{63}(\text{n},\alpha)\text{Co}^{60}$	5.11e-17	5.09e-17	5.05e-17	1.00	1.01
$\text{Fe}^{54}(\text{n},\text{p})\text{Mn}^{54}$	5.56e-15	5.51e-15	5.51e-15	1.01	1.01
$\text{Ni}^{58}(\text{n},\text{p})\text{Co}^{58}$	7.17e-15	7.58e-15	7.46e-15	0.95	0.96
$\text{U}^{238}(\text{n},\text{f})\text{Cs}^{137} \text{ Cd}$	2.74e-14	2.70e-14	2.76e-14	1.01	0.99
$\text{Np}^{237}(\text{n},\text{f})\text{Cs}^{137} \text{ Cd}$	2.75e-13	2.14e-13	2.49e-13	1.29	1.10
$\text{Co}^{59}(\text{n},\gamma)\text{Co}^{60}$	4.24e-12	5.01e-12	4.27e-12	0.85	0.99
$\text{Co}^{59}(\text{n},\gamma)\text{Co}^{60} \text{ Cd}$	1.97e-12	1.89e-12	1.96e-12	1.04	1.01

Table 15 (continued)

Comparison of Measured, Calculated, and Best Estimate  
Reaction Rates at the Surveillance Capsule Center

## Surveillance Capsule S

Reaction	Reaction Rate [rps/atom]			M/C	M/BE
	Measured	Calculated	Best Estimate		
$\text{Cu}^{63}(\text{n},\alpha)\text{Co}^{60}$	4.34e-17	4.25e-17	4.21e-17	1.02	1.03
$\text{Fe}^{54}(\text{n},\text{p})\text{Mn}^{54}$	4.42e-15	4.66e-15	4.45e-15	0.95	0.99
$\text{Ni}^{58}(\text{n},\text{p})\text{Co}^{58}$	5.81e-15	6.43e-15	6.05e-15	0.90	0.96
$\text{U}^{238}(\text{n},\text{f})\text{Cs}^{137} \text{ Cd}$	2.19e-14	2.33e-14	2.24e-14	0.94	0.98
$\text{Np}^{237}(\text{n},\text{f})\text{Cs}^{137} \text{ Cd}$	2.30e-13	1.88e-13	2.06e-13	1.22	1.12
$\text{Co}^{89}(\text{n},\gamma)\text{Co}^{60}$	3.29e-12	4.36e-12	3.32e-12	0.75	0.99
$\text{Co}^{89}(\text{n},\gamma)\text{Co}^{60} \text{ Cd}$	1.56e-12	1.70e-12	1.56e-12	0.92	1.00

**Table 16**  
**Comparison of Calculated and Best Estimate**  
**Exposure Parameters at the Surveillance Capsule Center**

**Time Averaged Exposure Rates**

	$\phi(E > 1.0 \text{ MeV}) \text{ [n/cm}^2\text{-s]}$		Uncertainty	BE/C
	Calculated	Best Estimate		
Capsule V	1.32e+11	1.13e+11	7%	0.86
Capsule R	1.26e+11	1.30e+11	6%	1.03
Capsule T	7.79e+10	8.11e+10	6%	1.04
Capsule S	6.78e+10	6.62e+10	6%	0.98

	Iron Atom Displacements [dpa/s]		Uncertainty	BE/C
	Calculated	Best Estimate		
Capsule V	2.40e-10	2.05e-10	9%	0.86
Capsule R	2.30e-10	2.37e-10	7%	1.03
Capsule T	1.36e-10	1.40e-10	7%	1.03
Capsule S	1.19e-10	1.16e-10	7%	0.97

**Integrated Capsule Exposure**

	$\Phi (E > 1.0 \text{ MeV}) \text{ [n/cm}^2\text{]}$		Uncertainty	BE/C
	Calculated	Best Estimate		
Capsule V	5.87e+18	5.03e+18	7%	0.86
Capsule R	1.02e+19	1.05e+19	6%	1.03
Capsule T	1.69e+19	1.76e+19	6%	1.04
Capsule S	3.64e+19	3.55e+19	6%	0.98

	Iron Atom Displacements [dpa]		Uncertainty	BE/C
	Calculated	Best Estimate		
Capsule V	1.07e-02	9.15e-03	9%	0.86
Capsule R	1.85e-02	1.91e-02	7%	1.03
Capsule T	2.94e-02	3.04e-02	7%	1.03
Capsule S	6.38e-02	6.22e-02	7%	0.97

### 3.5 COMPARISON OF MEASUREMENTS AND CALCULATIONS

In this section, comparisons of the measurement results from the four surveillance capsules withdrawn to date with the corresponding analytical predictions at the measurement locations are provided. These comparisons are given on two levels. In the first instance, calculations of individual sensor reaction rates are compared directly with the corresponding values obtained from the measured specific activities. In the second case, calculations of fast neutron exposure rates in terms of  $\phi(E > 1.0 \text{ MeV})$  and dpa/s are compared with the best estimate results obtained from the least squares evaluation of the three capsule dosimetry results. These two levels of comparison yield consistent and similar results with all measurement to calculation comparisons falling within the 20% limits specified as the acceptance criteria in Regulatory Guide 1.190.

In the case of the direct comparison of measured and calculated sensor reaction rates, the M/C comparisons for fast neutron reactions range from 0.78–1.32 for the 19 samples included in the data set. In the comparisons of best estimate and calculated fast neutron exposure parameters, the corresponding BE/C comparisons range from 0.85 –1.04 for the four surveillance capsules withdrawn to date.

Based on these comparisons, it is concluded that the data comparisons validate the use of the calculated fast neutron exposures provided in Section 3.2 of this report for use in the assessment of the condition of the materials comprising the beltline region of the R. E. Ginna reactor pressure vessel.



Table 17  
Comparison of Measured and Calculated Neutron Sensor Reaction Rates  
For In-Vessel Surveillance Capsules V, R, T, and S

Capsule	M/C Ratio					Average	% std dev
	Cu-63(n, $\alpha$ )	Fe-54(n,p)	Ni-58(n,p)	U-238(n,f)	Np-237(n,f)		
V	1.02	0.93	0.78	0.89		0.91	10.9
R	1.01	1.01	0.93	0.98	1.32	1.05	14.8
T	1.00	1.01	0.95	1.01	1.29	1.05	12.7
S	1.02	0.95	0.90	0.94	1.22	1.01	12.7
<b>Average</b>	<b>1.01</b>	<b>0.97</b>	<b>0.89</b>	<b>0.96</b>	<b>1.28</b>	<b>1.01</b>	<b>13.3</b>
<b>% std dev</b>	<b>0.8</b>	<b>4.2</b>	<b>8.4</b>	<b>5.5</b>	<b>3.9</b>		

Note: The average and % std dev values in bold face type represent the average and standard deviation of the entire 19 sample threshold foil data set.

Table 18  
Comparison of Best Estimate and Calculated Fast Neutron Exposure Rates  
For In-Vessel Surveillance Capsules V, R, T, and S

Capsule	BE/C Ratio	
	Neutron Fluence	Iron Atom Displacements
V	0.86	0.86
R	1.03	1.03
T	1.04	1.03
S	0.98	0.97
<b>Average</b>	<b>0.98</b>	<b>0.97</b>
<b>% std dev</b>	<b>8.7</b>	<b>8.6</b>